The Surface Force Balance: Direct Measurement of Interactions in Fluids and Soft Matter

Hannah J. Hayler, Timothy S. Groves, Aurora Guerrini, Astrid Southam, Weichao Zheng, and Susan Perkin

Physical and Theoretical Chemistry Laboratory, Department of Chemistry, University of Oxford, South Parks Road, Oxford, OX1 3QZ, UK.

E-mail: susan.perkin@chem.ox.ac.uk

Last compiled: Wednesday 31st January, 2024 (11:57)

Abstract. Over the last half-century, direct measurements of surface forces have been instrumental in the exploration of a multitude of phenomena in liquid, soft, and biological matter. Measurements of van der Waals interactions, electrostatic interactions, hydrophobic interactions, structural forces, depletion forces, and many other effects have checked and challenged theoretical predictions and motivated new models and understanding. The gold-standard instrument for these measurements is the *surface force balance*, or *surface forces apparatus*, where interferometry is used to detect the interaction force and distance between two atomically smooth planes, with 0.1 nm resolution, over separations from about 1 µm down to contact. The measured interaction force *vs.* distance gives access to the free energy of interaction across the fluid film; a fundamental quantity whose general form and subtle features reveal the underlying molecular and surface interactions and their variation. Motivated by new challenges in emerging fields of research, such as energy storage, biomaterials, non-equilibrium and driven systems, innovations to the apparatus are now clearing the way for new discoveries. It is now possible to measure interaction forces (and free energies) with control of electric field, surface potential, surface chemistry; to measure time-dependent effects; and to determine structure *in situ*. Here, we provide an overview the operating principles and capabilities of the surface force balance with particular focus on the recent developments and future possibilities of this remarkable technique.

Keywords: Surface Force Balance, Forces, Friction, Interactions, Thin films

Submitted to: *Rep. Prog. Phys.*

1. Introduction: from intermolecular to collective interactions and surface forces

Many research problems in the physical sciences involve exploring the manner in which interactions between atoms and molecules collectively determine the surface and inter-particle interactions of macroscopic materials. Commonplace observations such as the slipperiness of seaweed, the shear thickening of corn starch, or a spider scaling a wall have their origin in subtle molecular and electronic effects and involve non-classical physics. [1, 2] The span of lengthscales and diversity of materials involved in these questions naturally leads to crossing of traditional disciplinary boundaries including *soft matter*, *interface science*, *liquid matter*, *colloid science*, *nanoscience*, *tribology*, and *biomaterials*. Beyond matters of curiosity, current research questions are focussed on our energy revolution and recovery of the environment – how can we optimise electrolyte-electrode interfaces in batteries using Earth-abundant materials? [3, 4] And how can we aggregate micro-plastics for filtration from waste water? [5, 6, 7] A multitude of urgent research problems such as these require us to delve into the rich and complex origins of molecular and surface interactions.

A fascinating aspect of the interactions between macroscopic particles is the dramatic range of timescales and lengthscales emerging from apparently "simple" molecular forces, and the spectrum of effects observed. First, the *scaling* of interactions can vary drastically from molecular pair interactions to bulk materials. For example the weak van der Waals interaction between two molecules as a function of their separation, $u(r)$, scales with separation distance as $u(r) \sim 1/r^6$ and so is short ranged and acts essentially between nearest neighbours only. Yet these forces combine to drive long-range interactions between macroscopic bodies, $U(r)$, such as the attraction between oil droplets in water with $U \sim 1/r$, [8] or even "quantum levitation". [9] A second feature emerging from the scale-up from molecular pair interactions to *ensembles of interacting molecules* is the central importance of statistical effects and *entropy-driven* outcomes. In this category are polymer depletion forces, [10] electrostatic screening and double layer forces, [11] and more exotic observations such as attractive forces driven by correlations between like-charged ions. [12] On scaling molecular interactions to ensembles, long timescales can also emerge. Processes occurring over molecular dimensions in condensed phases under thermal conditions typically have timescales of $\sim 10^{-12}$ s; once scaled to motion over typical colloidal, biological or polymeric lengthscales the relevant timescales can be $\sim 10^{-3}$ s to 1 s, or slower. That is to say, rapid molecular motions give rise to effects that we can see in real time. [13] Taken together, these collective interactions are of central importance across all of the physical sciences: they determine the spontaneous formation and dispersal of membraneless biomolecular condensates, [14] the energy-cycling of ions in and out of battery electrodes, the formation of water droplets in clouds, and multitudes of other material processes. To interrogate these collective effects it is often of great use to make measurements of the *force* between particles or surfaces as a function of their separation distance across the fluid medium of interest.

What do we learn from measurements of surface forces? Most fundamentally, a force measured quasi-statically (reversibly) is the negative gradient of the free energy (the energy available to do work), so measuring a force over a distance gives access to the free energy difference between the two states. In an experiment at constant temperature and pressure this is a Gibbs energy. The free energy difference when surfaces approach across a medium will depend on medium-dependent quantities (*e.g.* liquid nano-structure, ionic screening, polymer radius of gyration), and surface-dependent quantities (*e.g.* surface charge, surface hydrophobicity). [15] With the aid of theoretical models, the force *vs.* distance measurement can be interpreted to give insight into each of these. In this way, direct measurement of surface forces is a powerful route to interrogate mechanisms and properties which are difficult to access in other ways.

Experimental measurements of surface interactions have been made for hundreds of years, from da Vinci's detailed analysis of frictional interactions [16] all the way to the prototypical force-measuring devices reported by Derjaguin [17] and by Overbeek [18] in the early and mid 20$^{\text{th}}$ Century. However it was the transformative innovations of Anita Bailey and J. S. Courtney-Pratt [19] that opened the way for quantitative measurements at the sub-nanometric (molecular) scale. Their detailed investigations into the origin of adhesion and friction were reported in 1955; these constitute the first use of optical interference to determine the separation distance between mica surfaces arranged in crossed-cylindrical geometry, and simultaneous detection of their interaction force via spring deflection.

After Anita Bailey's pioneering apparatus, further development by Tabor and Winterton [20] led to the formulation of the instruments later called the surface forces apparatus (SFA) and the surface force balance (SFB). These instruments were first applied to make direct measurements of the van der Waals force between macroscopic bodies in air[8] then much innovated by Jacob Israelachvili for measurements of forces in aqueous and non-aqueous solutions [21, 22] and by Jacob Klein [23], Steve Granick, and others, to investigate the role of polymers and soft matter in mediating surface interactions[24, 23, 25]. Herein, we will refer to these force-measuring instruments as *surface forces apparatuses* (SFAs) and *surface force balances* (SFBs) interchangeably.

The invention of the SFB, for direct measurements of the interaction between macroscopic bodies as a function of their separation distance across any fluid medium of interest, brought an extraordinary period of exploration and discovery over subsequent decades. The first measurements were made of van der Waals forces across air; [20] osmotic forces in electrolytes (electrostatic double layer forces); [26] hydrophobic attractions between non-polar materials immersed in water; [27] and depletion forces due to entropic exclusion of polymer chains. [10] Forces arising from dynamic or irreversible processes have also been studied using the SFB, to uncover energy dissipation mechanisms in many systems. An example is the measurement of friction forces: a friction cycle might involve lateral motion of one surface back-and-forth such that the final position of the surfaces is identical to the starting position. In this case the integrated force required to induce the cyclic motion corresponds entirely to dissipated

frictional energy. [28, 29] Shear (friction) forces due to surface-adsorbed or surface-grafted materials such as lipids, polymers, and polyelectrolyte brushes have been measured, from which the relation between molecular properties and lubrication or energy dissipation can be inferred. [30, 31] Another example is the measurement of viscous forces arising from the flows occurring in fluid as the surfaces move together. Velocity-dependence of (irreversible) surface forces can be interpreted in terms of the fluid drainage to determine, for example, slip boundary conditions or fluid viscosity in nanoscale films. [32, 33]

Whereas 20$^{\text{th}}$ century research questions in this field could be characterised by a wish to understand equilibrium structure and forces, research questions in the 21$^{\text{st}}$ century are often concerned with systems out of equilibrium, dynamic processes, and characterising the passage between states; the SFB is rising to this challenge. The measurement of surface forces is as important as ever, as the forefront of research in many disciplines from medicine to geology reaches the nanoscale: drug delivery now involves 'nanoparticles' targeted to interact with interfaces in specific ways [34]; energy storage involves battery materials engineered at the nanoscale to optimise energy density and cycling dynamics; [35] and micro-electronic devices now call for the fine-tuning of friction forces at a molecular level. [36] These current questions demand molecular-level insights into surface interactions and the SFB has evolved in many ways to respond to the new challenges.

With this review we aim to introduce the reader to the SFB and outline how it can be used to obtain insight in a range of research fields. We begin in section 2 with an overview of the central principles of the SFB. In section 3, we describe adaptations of the SFB, each designed to address a particular research question or system. In section 4, we look to the future: how might this remarkable 'chameleon' instrument assist as we face the research questions of our times?

2. The SFB: an optical and mechanical apparatus enabling model investigations of interaction forces across fluids

The SFB allows direct measurement of the interaction force between two macroscopic bodies – usually mica sheets laid upon cylindrical lenses and arranged in crossed-cylinder configuration – as a function of their separation distance across a fluid medium. White light incident perpendicular to the axes of the crossed-cylinders (radius ~ 1 cm) undergoes multiple reflections between mirrors on the back face of each mica sheet, resulting in multiple-beam interference with a spectrum consisting of *fringes of equal chromatic order* (FECO). [37, 19, 38] From the FECO spectrum the geometry of the interacting surfaces can be determined, including the distance of closest approach of the crossed cylinders, D, and (from the change in FECO positions with displacement) the force between them. This setup is shown schematically in figure 1, while examples from the range of systems that may be studied using the SFB are shown in figure 2 and the main features are elaborated below.

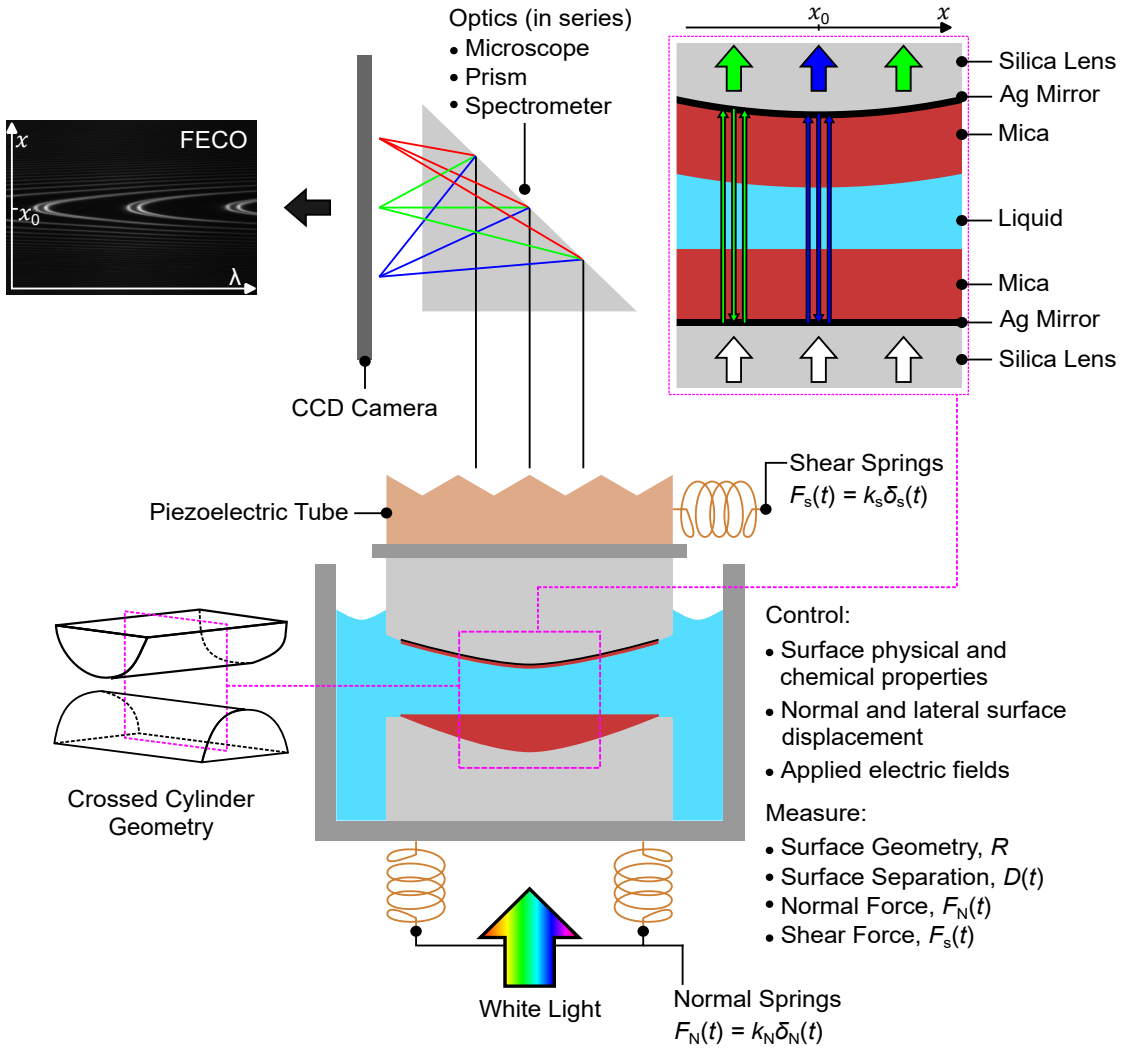

Figure 1. Operating principles of the basic surface force balance (SFB). White light is passed through the bottom lens into the interferometric cavity. Wavelengths that constructively interfere pass through the top lens to the spectrometer and then the camera, yielding fringes of equal chromatic order (FECO). The FECO are used to determine surface separation and radius of curvature of the lenses using the position of the fringes in wavelength, λ. Normal and shear springs with spring constants k_{N} and k_{s} are used to determine the normal and frictional forces, respectively.

2.1. Mica substrates

Ruby muscovite mica is the most common substrate for surface force measurements with the SFB owing to its near-ideal cleavage along the basal plane, allowing large area sheets of micrometric thickness to be prepared with no steps in the crystal plane on either face. Mica is a phyllosilicate clay mineral of lamellar crystals containing two tetrahedral silicate (SiO_4) layers either side of an octahedral aluminium oxide (AlO_6) layer. Al substitutions in the Si layer cause a residual negative charge which is neutralised by a layer of K^+ ions; these act to bind the lamellar sheets together. [39] The K^+ ionic plane is the cleavage plane, along which mica can be split to reveal macroscopic areas of

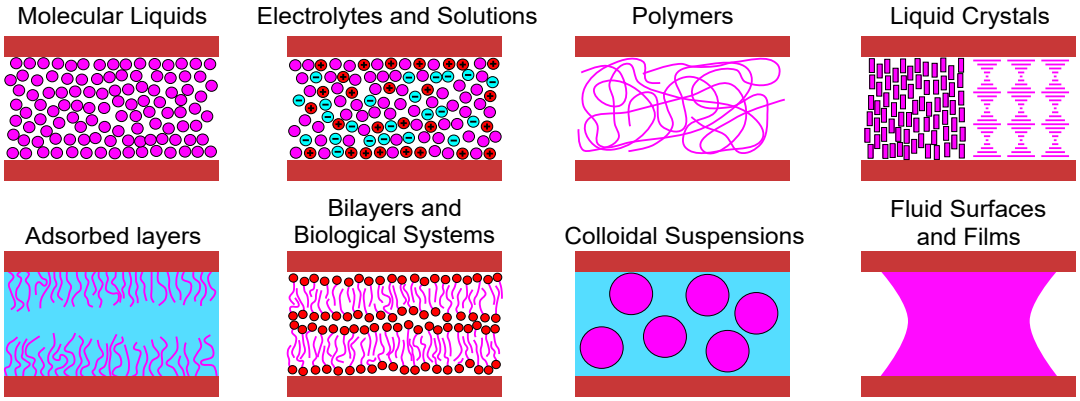

Figure 2. Illustration of the range of systems that may be studied using SFB.

fresh atomically-smooth (step-free) crystal surface. To use mica as a substrate for SFB measurements, a single step-free crystalline facet spanning the whole area of two lenses must be prepared, typically with a thickness of 1-4 µm. The delicate art of achieving this has been described previously. [40, 41] Many substrates other than mica have been employed, including many metallic surfaces (some mentioned below) as well as dielectrics such as silica. Studies of silica, in particular, allow for a comparison between the (chemically and topologically) uniform mica mineral and the rough and chemically heterogeneous silica surface.[42]

2.2. Crossed-cylinder geometry

The use of atomically-smooth crossed-cylinders creates a 'single asperity' contact which is geometrically equivalent to a sphere approaching a plane. The advantages of this geometry are that (i) it is well defined and therefore measurements can be directly compared to calculations; (ii) unlike the geometry of parallel plates, it can readily be set up in a geometrically ideal way with normal laboratory equipment and conditions; and (iii) crystalline lamellar sheets, *e.g.* mica, can be laid across the cylindrical lenses without wrinkles (which, as explained by Gauss's *theorema egregium*, cannot be achieved on a sphere), allowing for atomically-smooth crystals of identical composition on the two surfaces. Such ideally-smooth surfaces open the way to measurements involving large areas of interaction, *i.e.* large radius of curvature for the crossed-cylinders: in typical SFB experiments the cylindrical lenses have diameter 1 cm and radius of curvature 1 cm, each coated with a back-silvered mica sheet of area ~ 0.5 cm^2. The advantage in working with large (macroscopic) interacting surfaces is that the absolute experimental resolution in force – which is determined by the spring constant and noise level of the instrument and is typically 10^{-7} N – corresponds to a very fine resolution in interaction energy per unit area (about 10^{-6} J m^{-2}).

2.3. Fringes of Equal Chromatic Order

As white light is passed through the interferometric cavity formed by the silver-mica-medium-mica-silver stack, only those wavelengths that constructively interfere between the two silver mirrors will pass through the cavity to the spectrometer. The emerging wavelengths, once separated in the spectrometer, are observed as multiple beam interference fringes known as *fringes of equal chromatic order* (FECO) that are curved as a result of the contact geometry (see figures 1 and 3). Due to the birefringence of mica, the FECO can appear as singlets or doublets (depending on the crystallographic alignment of the mica surfaces, see Figure 3(b) and (c)). [43] FECO alternate between odd and even order fringes in accordance with their refractive index dependence; see figure 3(a) and section 2.4. [38]

The FECO spectrum gives a direct view of the confined region and can be analysed to provide information about many aspects of the confined film, the surfaces, and their interaction (see Figure 4). In a typical experiment the mica surfaces are first brought into contact in dry gas or air, where the fringes are observed to flatten due to adhesion between the mica sheets causing small deformations away from the crossed-cylindrical geometry (Figure 4A). The positions (wavelengths) of the FECO fringes at this mica-mica contact are calibrated as the point of zero surface separation. From the absolute wavelengths at this point, the thickness of the mica can also be determined. In a typical experiment, the mica surfaces are then separated and a fluid of interest is injected: either as a droplet held between the mica-coated lenses, or to fill the whole cell within which the lenses are held. The mica surfaces can then be brought towards one another again and the positions of the FECO can be used to determine the absolute surface separation – relative to the air calibration – with a precision of 0.1 nm and accuracy of 0.1 – 1.0 nm depending on the details of the experiment. The radius of curvature can also be determined precisely from the shape of the FECO *i.e.* the x-direction in figure 1, allowing for direct comparison across experiments and different confinement geometries (via the *Derjaguin approximation*). [15]

This optical detection method of determining the surface separation in fact measures the *optical* thickness, *i.e.* a refractive index-weighted quantity. If the refractive index (RI) of the confined medium is uniform and well defined, this simply reduces to a measure of thickness (as described above). If the medium of interest consists of anisotropic components (*e.g.* liquid crystals), or there exist multiple phases with dielectric or RI contrast, or the RI varies with the degree of confinement, these features can be observed directly using the FECO. This gives direct visualization *in situ* of events such as capillary condensation, [44, 45] phase separation, [46] liquid crystal reorientation and alignment, [43, 47, 48, 49, 50, 51, 52] as well as quantitative insights into the surface coverage of polymers. [53]

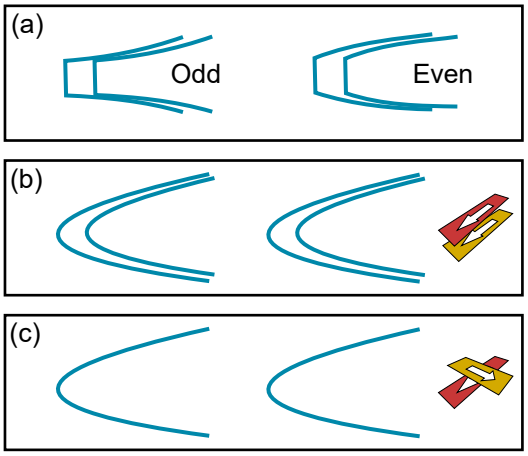

Figure 3. Schematic view of fringes of equal chromatic order. (a) Flattened FECO at the contact position, highlighting the shapes of the odd and even fringes. (b) FECO can appear as doublets if the mica optical polarisation axes are parallel. (c) If the mica optical polarisation axes are perpendicular, the fringes appear as singlets. [43]

2.4. Image analysis of the FECO

The FECO, or 'fringes', are recorded using a CCD camera which captures images at a typical frame rate of 5 FPS, although this can be much higher when required for dynamic studies. [54] The images can then be analysed to determine the surface separation, refractive indices, geometry of confinement, and interaction force.

If the medium of interest is confined between two muscovite mica surfaces of identical thickness, the system can be described as a symmetric three-layer interferometer. Israelachvili [38] derived the following formula to determine the surface separation, D, in a symmetrical three-layer interferometer,

$$\tan(k\mu_{\text{medium}}D) = \frac{2\bar{\mu}\sin\theta}{(1+\bar{\mu}^2)\cos\theta \pm (\bar{\mu}^2-1)}, \tag{1}$$

where $k = 2\pi/\lambda$, $\pm$ depends on whether λ belongs to an odd or even fringe, and

$$\bar{\mu} = \frac{\mu_{\text{mica}}}{\mu_{\text{medium}}} \qquad \theta = \frac{n\pi\Delta\lambda_n}{\lambda_n} \qquad n = \frac{\lambda^0_{n-1}}{\lambda^0_{n-1}-\lambda^0_n} \tag{2}$$

when μ_i is the refractive index of layer i, n is the fringe order, λ^0_n and λ^0_{n-1} are the wavelengths of the fringes n and $n-1$ at $D = 0$ nm, respectively. If $D \neq 0$ nm, the wavelength of the n-fringe shifts to λ_n by $\Delta\lambda_n = \lambda_n - \lambda^0_n$. In this case of a symmetric interferometer, the FECO alternate between odd and even order fringes, with their profiles differing at small distances. [38] Odd fringes are not sensitive to the RI of the medium at short distances, whereas even fringes depend on the RI of the intervening medium:

$$D = n\Delta\lambda_n/2\mu_{\text{mica}}\ (n \text{ odd}) \qquad D\mu^2_{\text{medium}} = n\Delta\lambda_n\mu_{\text{mica}}/2\ (n \text{ even}). \tag{3}$$

By tracking the shift in an odd fringe, D can be determined directly. [38]

Surface separation is measured relative to mica-mica direct contact ($D = 0$ nm) as calibrated at the start of each experiment. The calibration is made by recording the wavelengths of two adjacent fringes *e.g.* p and $p-1$ with wavelengths λ_p^0 and λ_{p-1}^0 in figure 4(a). When a medium sits between the lenses, as in figure 4(b), the position of the p-fringe shifts to λ_p by $\Delta\lambda_p = \lambda_p - \lambda_p^0$. By tracking λ_p as the lenses approach or retract, the surface separation can be determined.

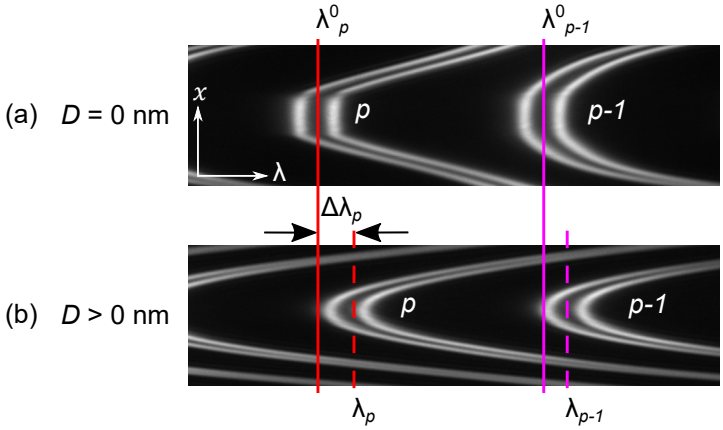

Figure 4. FECO fringe pattern example in (a) air and in (b) liquid. The fringes appear as doublets due to the birefringence of mica. The left-most odd fringe is termed the 'p-fringe'. In air, the flattening of the fringes indicates clean mica-mica contact. In liquid, the p-fringe is shifted by $\Delta\lambda_p$ relative to the p-fringe in air, with the shift corresponding to the surface separation. Here, the wavelength at the mid-point of each doublet is marked. Alternative positions can also be used *e.g.* the apex of the left-hand fringe of the doublet.

Using multiple beam interferometry, the surface separation relative to the calibration can be measured with a precision of 0.1 nm, provided the optical setup is optimal. This is determined by factors such as the light alignment and collimation, condition of the mica surface, and the silver thickness, purity and smoothness. [38]

2.5. Determining the surface forces by spring deflection

The SFB can be used to measure both normal and lateral forces across confined films using two sets of leaf springs (see figure 5, parts C and E).

2.5.1. Normal Forces. The bottom lens sits on a pair of parallel leaf springs, as in figure 5, with spring constant, k_{N}. When the lenses are at very large separation they experience no interaction force, i.e. $F_{\mathrm{N}} = 0$. The two surfaces are brought together using a three-stage mechanism: the coarse motor positions the lenses within about 1 µm, the fine motor via a differential spring mechanism positions to 1 nm, and a piezoelectric tube (PZT) allows positioning to 0.1 nm (see figure 5). Generally, measurements are conducted with the fine motor or PZT. The fine motor allows for a larger range of linear motion, however can introduce mechanical vibrations, whilst the PZT minimises

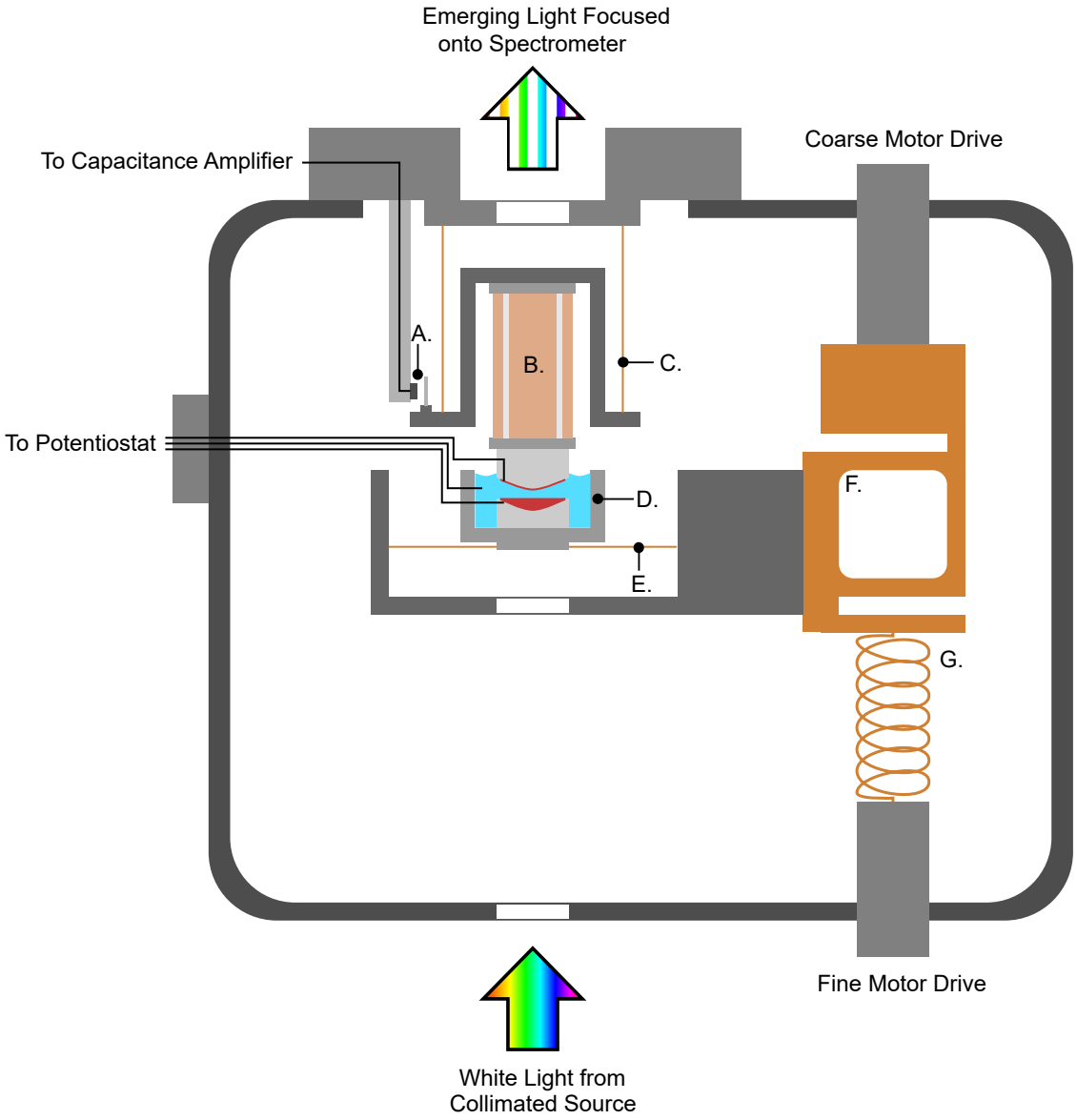

Figure 5. Basic mechanical setup of the SFB within the chamber (outermost dark grey square). Labels correspond to: **A**. air-gap capacitor. **B**. piezoelectric tube. **C**. shear leaf springs. **D**. bottom lens holder. **E**. normal leaf springs. **F**. stiff spring. **G**. helical spring.

vibrations but has a smaller range of motion. As the surfaces approach one another, an interaction force between them causes deflection of the spring. This deflection is detected via the FECO, and from this the (static and dynamic) interaction force can be calculated as follows.

The mechanics of the system can be understood by considering the equation of motion of the lower lens relative to the upper lens as follows[55]:

$$m\ddot{D} = F_{\rm N}(D) - k_{\rm N}\delta_{\rm N}(t) + F^h(D,\dot{D}) \tag{4}$$

where m is the mass of the bottom lens on the spring, $F_{\rm N}(D)$ is the equilibrium ($\dot{D}=0$)

force acting between the surfaces at separation D, k_{N} is the spring constant, $\delta_{\mathrm{N}}(t)$ is the deflection of the spring and $F^h(D,\dot{D})$ is the hydrodynamic force acting between the surfaces. It is noted that here we have assumed the hydrodynamic and equilibrium forces are independent and separable.

The spring deflection is measured using FECO fringes: if a constant velocity of approach of the top surface towards the bottom surface is imposed (see red dotted line in figure 6), then the spring deflection is equal to the deviation of the actual separation distance, $D(t)$, from a linear baseline of $(D_0 - vt)$:

$$\delta_{\mathrm{N}}(t) = D(t) - [D_0 - vt]. \tag{5}$$

Thus the directly measured force is simply: $F_{\mathrm{N}}(t) = k_{\mathrm{N}}\delta_{\mathrm{N}}(t) = k_{\mathrm{N}}(D(t) - D_0 + vt)$. Under all normal conditions for SFB experiments, the intertial term in the equation of motion, $m\ddot{D}$, is negligible. Thus the instantaneous force acting between the surfaces resulting in the observed deflection of the spring, $F_{\mathrm{N}}(D,t) = k_{\mathrm{N}}\delta_{\mathrm{N}}(t)$, is determined by the equilibrium force and any viscous (hydrodynamic) contribution. In crossed-cylinder geometry the hydrodynamic drainage force is equivalent to that between a sphere and a flat plate[55], and so we have:

$$F(t) = k\,(D(t) - D_0 + vt) = F_{\mathrm{N}}(D) + 6\pi\eta R^2\frac{\dot{D}}{D} \tag{6}$$

In many cases where the approach speed $\dot{D}$ is very slow and/or the fluid viscosity is low the hydrodynamic term is negligible and the directly measured force, $F(t)$ is equal to the equilibrium normal surface force $F_{\mathrm{N}}(D)$. For example experiments in water with $R \approx 1$ cm and approach speeds of 1 nm/s viscous forces are negligible. However, when studying viscous fluids or when imposing higher approach speeds the additional time-dependent contribution must be included. A careful analysis of how this was performed in an ionic liquid studied over several orders of magnitude in approach velocity illustrated how this can be done.[33]

An experimental surface separation versus time profile is shown in figure 7(a), for the example of an ionic liquid confined between the mica surfaces and measured at an approach rate where viscous forces were negligible. The linear approach is fitted when $D > 40$ nm (in red). Below approximately 20 nm, $D(t)$ deviates from the linear baseline indicating the presence of surface interactions. The normal force is then determined, as in figure 6, and plotted against surface separation yielding the normal force-surface separation profile in figure 7(b). Using the SFB, normal forces can typically be measured with a resolution of 10^{-7} N [56].

2.5.2. Shear Forces. The SFA was adapted for simultaneous measurement of lateral and normal forces by Israelachvili's team, and this uncovered many aspects of the molecular mechanisms underlying friction and its relation to adhesion between surfaces.[57] Later, a method for ultra-sensitive detection of shear forces was implemented by Klein and Kumacheva[58], involving nanoscale lateral displacement of one surface using a sectored piezoelectric tube and fine detection of the resulting shear

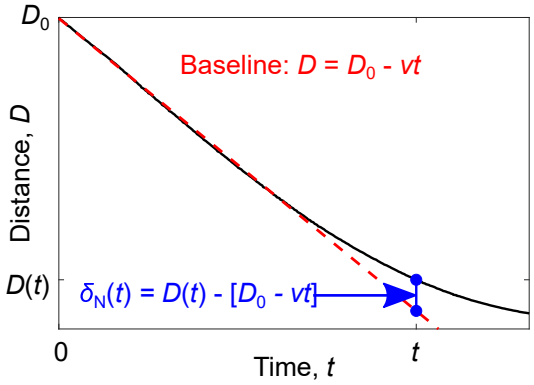

Figure 6. Distance, D, versus time, t, schematic. The black line shows the experimental $D(t)$ profile. When the lenses approach one another, the imposed motion is described by a linear baseline: $D = D_0 - vt$, that depends on the starting distance, D_0, approach velocity, v, and time. This baseline is shown in red. The deflection, $\delta_N(t)$, in blue is given by the difference between $D(t)$ and the linear baseline: $\delta_N(t) = D(t) - [D_0 - vt]$.

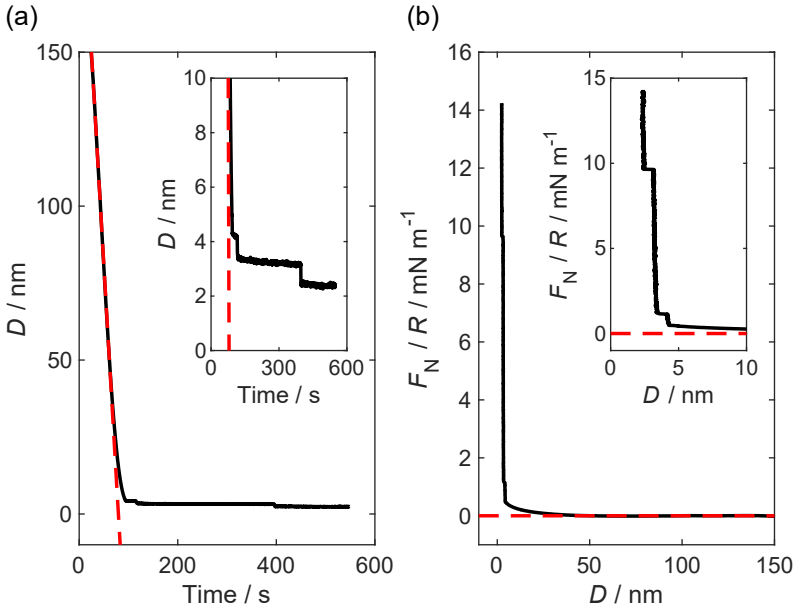

Figure 7. Examples of (a) distance-time and (b) force-distance profiles for an ionic liquid. (a) Surface separation, D, versus time plot in black. When $D > 40$ nm the surface separation can be fitted linearly with time (red dashed line). A series of steps are observed when $D < 10$ nm, shown in the inset. The difference between the black and red plots in (a) gives the deflection needed to calculate the force, F_N. This is normalised by the radius of curvature of the lenses, R, and plotted as a function of D as in (b). The red dashed line in (b) shows the linear fit from (a) and corresponds to $F_N = 0$ mN. The forces at $D < 10$ nm are shown in the inset.

coupling using a hanging spring mechanism; see figure 5. The sectored piezoelectric tube, upon which the top lens is mounted, is used for both normal and lateral motion. By applying equal voltage to all outer sectors, and to the inner sector, the tube

expands/contracts normally. Lateral motion is achieved by applying equal and opposite potentials to two opposing outer sectors so that one contracts whilst the other expands. A signal at twice the frequency of that applied to the outer sectors can be applied to the inner sector of the piezoelectric tube in order to offset any bowing of the trajectory and ensure the shearing motion of the top lens is parallel to the bottom lens. Shear forces can be measured while the lenses are at fixed separation distance, D, or simultaneously with normal translation. Provided the normal approach velocity is much smaller than the shearing velocity, the surface separation can be assumed constant during one shearing cycle; the latter method has recently been described in detail [59].

Vertical leaf springs, with spring constant k_{s}, deform if any shear forces are present between the two surfaces. The deformation is detected by measuring the change in capacitance across an air-gap capacitor formed between a capacitance probe and a mirror-polished steel flag rigidly attached to the shear spring (figure 5, part A).

3. Adaptions to the SFB have allowed diverse physical and chemical phenomena to be resolved

The SFB has been adapted in many ways to allow measurement of different features of surface forces and properties of confined and interfacial fluids; we summarise some of these in Figure 9. One of the earliest efforts to measure the force and separation distance between approaching surfaces using interferometry was by Derjaguin (Figure 9(a)), presented at a remarkable cold war Faraday Discussion meeting[17]. This was followed just a year later by the apparatus of Bailey[19], which was refined by Tabor[60] and developed further and applied to a great many systems by Israelachvili [61, 38, 62, 63, 26, 21, 64, 65, 66, 22]. Many of the standard features of the SFB as used today, and as described in Section 2 , are essentially similar to these versions of apparatus reported more than 50 years ago. However advances in image and data capture, digital control, programmability, and analysis have allowed improvements in precision and resolution of distance measurement and access to fast processes. For example, Heuberger *et al.* [67] showed how the full interference pattern of a three-layer interferometer could be processed to determine surface topography in and out of contact. Later, Heuberger [68] modified the SFB to produce a fully automated instrument with measures to control both thermal and non-thermal drift (*e.g.* material creep), [69] known as the extended surface forces apparatus (eFSA). Recently, the SFA was miniaturised by Kristiansen *et al.* allowing for concurrent force measurements and spectroscopic studies. [70] Modifications allowing for the measurement of dynamic *shear* forces across confined liquid films were made by Klein and Kumacheva [58, 71]; this apparatus allowed for determination of mechanisms underlying friction and lubrication in systems involving adsorbed and grafted polymers, hydrated ionic systems, biological macromolecules and assemblies. Building on this delicate mechanism for detecting lateral forces, Lhermerout[59] showed that by simultaneously approaching and shearing the surfaces, further dynamic information can be obtained.

Improvements to the optical setup and data capture of the interference pattern have led to enhanced resolution and precision of SFB measurements in recent years. For example, it is now routinely possible to measure molecular-scale details such as oscillatory forces arising from water structure; a measurement which was challenging and even controversial in the past due to the stringent requirements of cleanliness and fine resolution[72]. An example of recent measurement clearly showing oscillations in force with a wavelength of 0.28 nm, attributed to water correlations (water structure), is shown in Figure 8. [73]

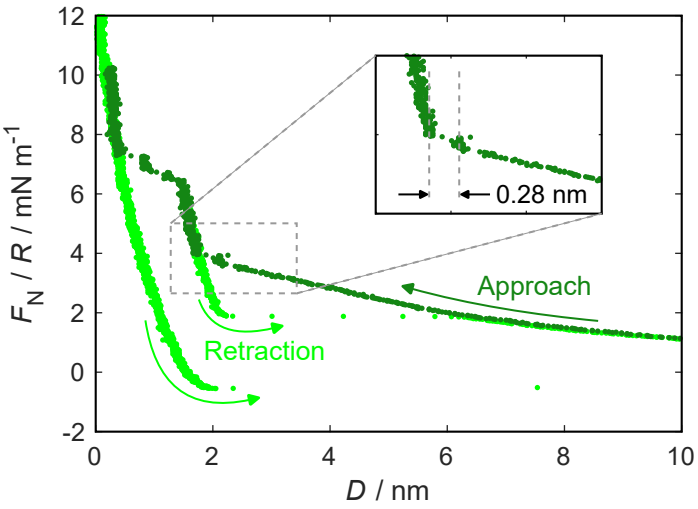

Figure 8. Force-distance profile as measured in aqueous 1 mM KCl, adapted from a work by Hallett *et al.* The results clearly show steps with dimensions of 0.28 nm, which are attributed to the successive squeeze-out of ordered layers of water from between the surfaces

Other adaptations of the SFB, as in Figure 9, involve variation to the path of the light and mirror arrangement, or substrate material, or electrochemical control. In this section we outline some of those key developments and describe the new insights into material and interfacial properties they have enabled.

3.1. Measuring forces with control of electrochemical potential and electric field

3.1.1. Applying controlled electric fields perpendicular to confined films A notable extension to the mica-mica SFB is that developed by Drummond [74] to allow for the application of controlled and well-defined electric fields at the nanoscale. In the device, shown schematically in Figure 9(c), the silver mirrors on the backs of the mica surfaces are used simultaneously as electrodes, in order that the electric field resulting from their electric potential difference is precisely perpendicular to the confined liquid film (i.e. is in the axial direction). The simplicity and elegance of this method, allowing for simultaneous determination of surface separation and surface forces while the electric field is applied, opens the way to many avenues for study of field-dependent effects in fluids. Since the electrodes are behind the mica sheets, which provide a dielectric barrier

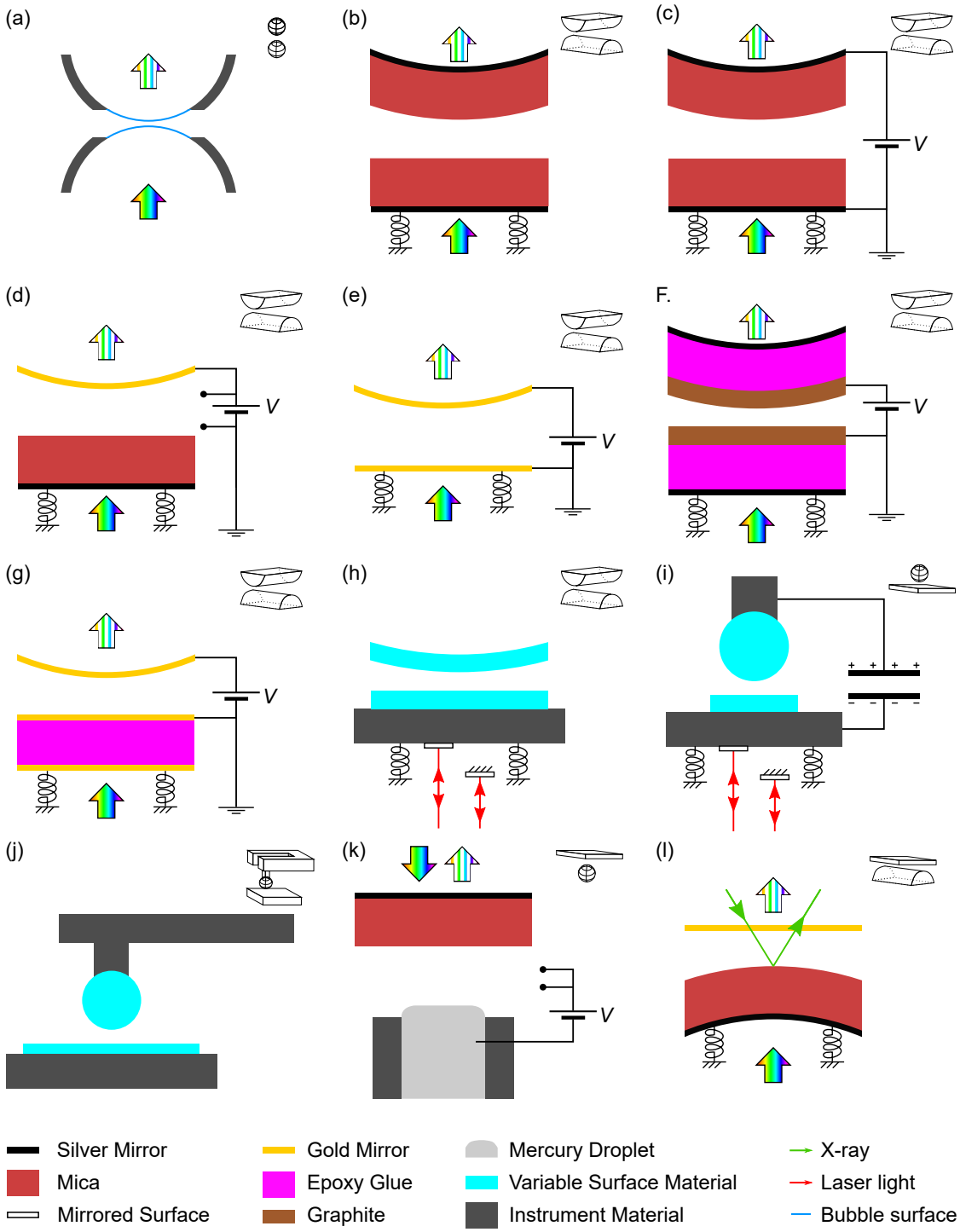

Figure 9. Examples of various adaptions of the surface force balance. From left to right and top to bottom: (a) Derjaguin's proto-SFA in which film thickness between gas bubbles was measured by interferometry, [17] (b) Mica-mica SFA, [19, 60] (c) Mica-mica electric field set-up of Drummond, [74] (d) Mica-gold asymmetric set-up of Klein, [75] (e) Gold-gold set-up of Perkin, [76] (f) Graphene SFA of Perkin, [77] (g) Triple gold SFA of Perkin, [78] (h) Two-beam interferometry SFA of Kurihara, [79] (i) Dynamic SFA used by the Charlaix group, [80, 81] (j) MicroMegascope pioneered by the Niguès group, [82] (k) Mercury-mica electric field set-up of Horn, [83] and (l) X-Ray SFA of Valtiner. [84] In each case, the geometry of confinement is shown in the top right hand corner.

between electrode and fluid of interest, the effect of well-controlled electric fields can be studied without interference of Faradic processes.

In particular, since the electrodes are separated by only a few micrometres (the thickness of the two mica sheets of typically 1-4 µm each and the nanometric liquid film), high electric fields can be generated with only modest applied voltage. For example, 20V applied between the electrodes at a separation of 5 µm leads to an electric field of $4 \times 10^6\ V\mathrm{m}^{-1}$. At such electric fields, the field energy and thermal energy densities become comparable and so the field is expected to influence molecular orientations and interactions[54].

An example of the control of surface interactions by application of electric fields has been reported by Drummond [74], where the lubrication properties of polyelectrolyte brush layers was shown to be switched when AC fields were applied across the interfacial film. A significant reduction was found in the friction forces at high loads when the field is applied, which is attributed to the collapsing of the polymer brush in the presence of an electric field as the solvation structure of the polymers reorganises; see Figure 10. Since then a similar technique was used by Perez-Martinez [76] in the characterisation of forces generated by the action of AC electric fields across electrolytes on the application of oscillating electric fields.

3.1.2. Control of surface electrical potential. One of the key limitations associated with the traditional mica-mica SFA is that mica is an insulator and its surface electrical potential cannot be directly controlled. [78] However, controlling surface potential is important for many real-life applications of confined systems *e.g.* electrolytes in energy storage devices. By replacing one mica surface for gold, surface potential can be controlled relative to an electrode in the bulk liquid and used to study metal-liquid interactions and surface forces with controlled electrode potential; Figure 9(d). Vanderlick *et al.* [85, 86, 87] provided crucial insight into the relationship between surface roughness of gold and optical resolution which Klein and Chai [75] built upon to successfully characterise aqueous electrolyte behaviour using a gold-mica setup.

While gold is a suitable candidate for this due to its high reflectivity, the surface roughness of directly deposited gold films made it incompatible for interferometric analysis or molecular-resolution studies. By adapting the template stripping method first proposed by Hegner *et al.* [88, 89], they were able to achieve smooth gold surfaces compatible with interferometric analysis. Additionally, straightforward modifications to the Au-mica system permits the incorporation of a classical three-electrode setup, [90, 91]. In an important fundamental study by Tivony *et al.*, Figure 11, this apparatus was used to test the applicability of constant potential and constant charge boundary conditions for the Poisson-Boltzmann model as applied to interaction forces across electrolyte solutions [92].

Another simple way to study a symmetric system of electrodes on both surfaces in direct contact with the fluid between is to remove the mica spacer completely to leave a single layer interferometer with gold acting as both mirror and electrode on both faces,

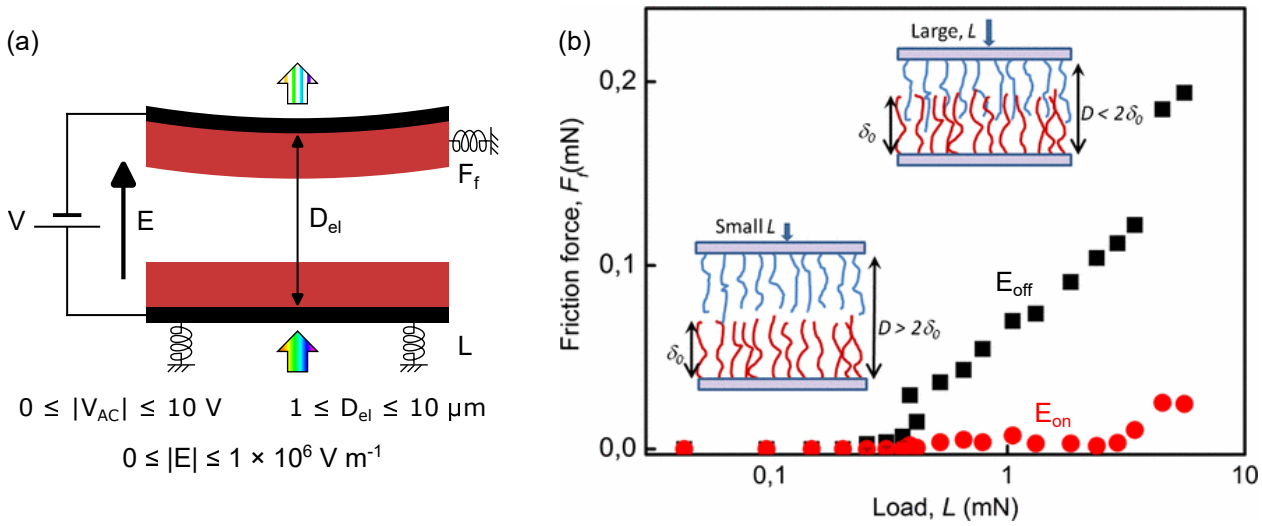

Figure 10. The electric field and shearing SFB set up and applications. (a): Set up of the electric field and shearing SFB. A potential difference V is applied between the two silver mirrors, separated by a distance D_{el} giving rise to an electric field E. Surface separations and normal load forces are measured by white light interferometry and by monitoring the deflection of a spring normal to the direction of the light. One surface may also oscillate orthonormally to the direction of the light, and is capable of applying a friction force F_f which may be measured by monitoring the deflection of a second spring. (b): Example results from the set up, showing the load dependence of friction force between mica surfaces coated with a a layer of PS_{36}-PAA_{125} with (red circles) and without (black squares) an externally applied electric field. At low L the PE layers oppose very small resistance to shear because of limited layer interpenetration. Lubrication is substantially worsened at larger loads. F_f is greatly reduced when the external field is applied (alternating square wave voltage, 450 Hz, 20 V p-p amplitude). Shear velocity $V = 0.3$ μm/s, and mica thickness is 4.018 µm. Reprinted figure with permission from C. Drummond, *Physical Review Letters*, 109, 154302, 2012. Copyright 2012 by the American Physical Society. [74]

as in figure 9(e). Because of the optical requirement that the space between the mirrors must be greater than about 1 µm to allow for interference fringes to appear in the visible range, this setup can only be used to study forces occurring at electrode separations beyond this distance. However the simplicity of the interferometer leads to very good resolution in relative distance for $D > 1$ μm and makes this setup ideal for measuring forces over micrometric length scales with control of surface potential. Another key benefit of this set-up is the precisely known electric fields between the surfaces: with no dielectric mica spacer to attenuate the field, the potential at the electrode-electrolyte interfaces is known precisely. In 2015, the method was used by Kristiansen *et al.* [49] where they applied the back-silvered mica to the cylindrical lens mica-side down, to produce a silver layer acting both as a mirror and an electrode. The system was used to measure the molecular forces and electro-optical properties of a confined nematic liquid crystal. A similar technique was later developed by Perez-Martinez *et al.* [76] in which gold was evaporated onto chromium coated cylindrical lenses. They performed

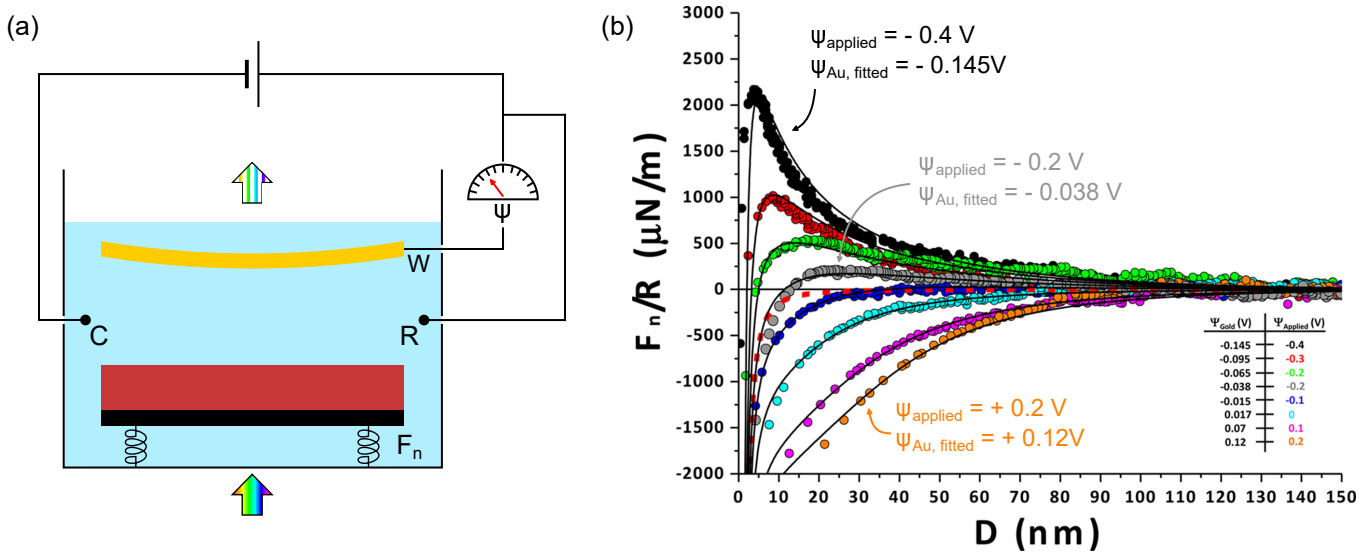

Figure 11. The Au-mica SFB set up and an example experiment. (a): Set up of the Au-mica SFB. Measurement takes place in a three electrode cell, with counter and reference electrodes immersed in solution, while the gold mirror acts as the working electrode. The applied potential ψ_{applied} for the working electrode may be chosen for each measurement. Surface separation and normal forces are measured by white light interferometry and by monitoring the deflection of a normal spring. (b): Example results from the set up. Forces are measured by approaching the gold and mica surfaces in the presence of water with no added salt (pH = 5.8). ψ_{applied} is varied and the resulting force profiles are fitted to the Poisson-Boltzmann equation to extract the potential on the gold surface $\psi_{\text{Au,fitted}}$. The mica surface has constant charge, while the gold surface has constant potential. At low negative potentials on the gold surface, charge reversal character is seen in the surface layer close to the gold, with longer-ranged attractive forces than would be expected from the van der Waals contribution alone. Reprinted with permission from J. Klein, G. Silbert, R. Tivony, and D. B. Yaakov, *Langmuir*, 31(47), 12845, 2015. Copyright 2015 American Chemical Society. [90]

measurements to quantify the surface forces generated by the action of electric fields across micrometric liquid films, revealing unexpected large repulsive forces evolving over long timescales. A similar observation was made by Drummond, who interpreted the repulsive forces arising when AC fields are applied across an electrolyte as due to differences in cation and anion diffusivity, which drive a build-up of charge between the surfaces and therefore ratcheting up of excess osmotic pressure over long times.[93]

3.1.3. Graphene SFB. Whilst the one-layer interferometer mentioned above works well for studies of electrically-induced effects at large separations, another method is needed in order to study nanometrically thin films confined between two identical electrode (conducting) surfaces. The trick of using mirrors (for interferometry) simultaneously as electrodes (for applying voltages) is not of use if the electrodes are to approach to nanometric separations; instead an ultra-smooth, optically transparent electrode must be found. Achieving the required level of smoothness (sub-nanometric roughness, at

least) of the electrode surface is challenging; standard transparent electrode materials like ITO were not suitable. One suitable material is graphene, and this method has been applied in constructing the 'graphene surface forces balance' (gSFB) in which layers of graphene acting as optically transparent electrodes are set apart from silver mirrors by a thin smooth layer of transparent epoxy as spacer. The gSFB is shown in Figure 9(f).

The gSFB allows face-to-face graphene-graphene interactions across air and liquid films to be studied. The double-transfer method developed by Britton *et al.* [94] produces chemically clean and molecularly smooth graphene-coated lenses that are suitable for force measurements and interferometry. The inherent conductivity of graphene also allows the forces to be measured as a function of surface potential. The resulting gSFB has also been used to directly measure single-layer and few-layer graphene surface energies in dry nitrogen and interfacial energies of few-layer graphene in water and electrolyte solution. Interestingly, the comparison between adhesion with single-layer and few-layer graphene provides a window into the 'van der Waals transparency' of graphene which will likely be important for many experiments and applications involving these and other 2-dimensional structures [77, 95].

3.1.4. Triple Gold Approach. Another method designed to achieve identical polarisable substrates with atomically smooth surfaces is the triple gold mirror SFB setup (Au3 SFB). This method, developed by van Engers *et al.* [78] and based on the work of Levins and Vanderlick [96], utilises a mica-free three-mirror interferometer where two template-stripped gold surfaces serve as confining surfaces, while a third gold mirror affords detection of thicknesses below the diffraction limit of light with nanometre resolution (see figure 9(g)). By using a triple gold setup, the surface potentials of the two gold electrode surfaces, each in contact with the electrolyte, can be controlled symmetrically or asymmetrically without the need to sacrifice optical resolution. In the Au3 setup, the key modifications are the use of two gold mirrors on one lens, which are separated by an epoxy spacer, and the use of template-stripped gold surfaces as the confining surfaces. Template-stripping the gold yields smooth surfaces with an RMS roughness of approximately 0.2 nm, which is significantly less than the roughness of gold films created by vapour deposition (approximately 1.2 nm RMS roughness [97]). Together, these modifications provide sub-nanometric optical resolution along with the advantages of an electrochemical setup. A rigorous method for interpretation of FECO fringes from this asymmetric multi-layer interferometer has been developed[78]. The symmetric control of surface potential opens the way to high resolution and direct studies of many electrolyte-electrode phenomena, such as the structure and dynamics of electrical double layers in different media under nanoscale confinement. Challenges remain, however, because of the complexity of the FECO spectrum arising from this interferometric setup meaning that direct view of the spectrum during an experiment does not give the same intuitive 'view' of the contact and all analysis must be performed *post hoc*.

3.1.5. The twin-path apparatus. The twin-path surface forces apparatus (SFA) was designed by Kurihara *et al.* [79] to study interactions between opaque substrates and/or liquids; Figure 9(h). Instead of using the conventional multiple beam interferometry and FECO to determine the surface separation, two-beam interferometry is used where the phase difference between two reflected light beams (one beam with a fixed path length and one with a path length that varies with the motion of the bottom sample holder) is monitored and the surface displacement can be calculated. Using the twin-path SFA, Fujii *et al.* were able to measure surface forces as a function of applied potential between platinum electrodes in 1 mM $HClO_4$. To date the twin-path SFA has been used to study lubricants between iron surfaces; [98] interactions between ice-silica [99] and the ice premelting layer-silica; [100] viscoelasticity of rubber-ice interfaces; [101] electrical double layer forces [102], and anion adsorption on gold electrodes. [103].

3.1.6. Mica-Mercury droplet system. An alternative method for accessing ultra-smooth metal surfaces, as necessary for investigation of electrode-electrolyte effects with sub-molecular resolution, is to use a liquid mercury electrode. Horn's laboratory developed a surface force apparatus for measuring the interaction between a mica surface and a liquid mercury electrode across an electrolyte (see figure 9(k)). The apparatus involved modifying the optics of the SFA allowing them to carry out measurements in reflection mode, so that a mercury droplet could be used both as an electrode and a reflective (but not transmitting) mirror.[104] This allowed one opaque surface to be studied, provided the surface was smooth and partially reflective. The other surface, which was mica in their experiments, must be optically transparent for the incident and reflected light to pass through. The Hg-mica SFA has provided elegant and insightful measurements directly testing fundamental aspects of the relation between surface potential and surface charge at electrode-electrolyte interfaces and the detailed validity of the Poisson-Boltzmann model for capturing interactions in aqueous electrolytes, a question of great generality and significance (see figure 12). [83]

3.2. Measuring time-dependent forces and dynamic effects

3.2.1. The Dynamic Surface Force Apparatus. The Dynamic Surface Force Apparatus (DSFA) was first developed by Restagno *et al.* [80, 81] to measure rheological properties of the matter confined between the two surfaces. In the DSFA, an oscillatory displacement of small amplitude is superimposed on a linear inwards ramp of one surface towards the other. Analysis of the static and dynamic response gives access to normal and dynamic forces that allow the rheology of the confined system to be studied. In the original device, absolute separation was measured using a capacitance sensor, while forces were obtained with a Nomarski interferometer that measured the deflection of a cantilever spring, as in figure 9(i). The device was recently updated to enable study in fluid baths (and hence allow investigations into more volatile systems) by replacing the capacitor with a second Nomarski interferometer. [105] The DFSA typically uses

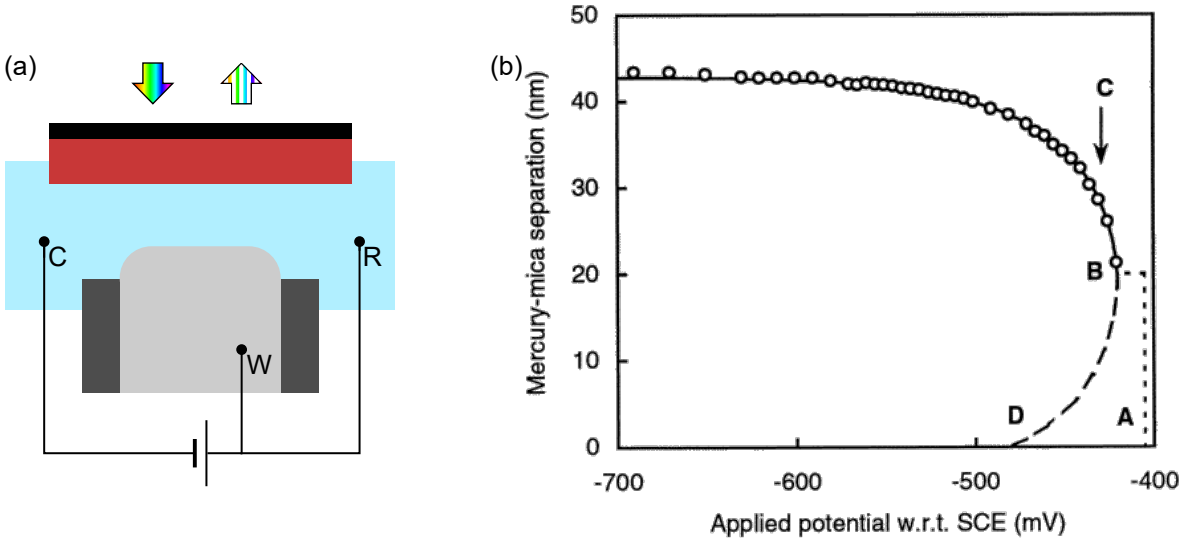

Figure 12. The Hg-mica SFB set up and an example experiment. (a): Set up of the Hg-mica SFB. Measurements take place in a three electrode cell, with counter and reference electrodes immersed in solution, while the liquid Hg surface acts as the working electrode. Separation between the mica and mercury surfaces is measured by white light interferometry following a reflection rather than transmission pathway. (b) Example results from the set up, validating the Poisson-Boltzmann (PB) equation. The mica surface becomes negatively charged on immersion in an electrolyte. If a negative potential is applied the Hg at constant pressure, the repulsion between the mica and Hg electrode causes the Hg surface to flatten and thus the film thickness to increase. The calculated separation resulting from a double layer repulsion force between two surfaces at constant pressure is shown by the solid black line, while measurements of the film thickness are shown by the circles. The excellent match between the data and the prediction validate the PB result. **A** shows the amount by which the PB curve is shifted to match the data, **B** shows the position of minimum-magnitude potential, **C** shows the point of zero electronic charge, and **D** shows the mica outer Helmholtz plane surface potential. Reprinted with permission from J. Connor and R. C. Horn, *Langmuir*, 17, 7194, 2001. Copyright 2001 American Chemical Society. [83]

a spherical bead, usually silica, approaching a flat surface. Importantly, as distances and forces are not measured by analysis of fringes of equal chromatic order, the surfaces are not required to be transparent or optically smooth. Since its design, the DSFA has been used to measure boundary flow on various surfaces, [106, 107, 108] the effect of elasticity on surface flow [109] and rheological properties of simple and complex fluids [110, 111], to name just a few examples.

3.2.2. MicroMegascope. The MicroMegascope (MiMes), developed by the Siria/Niguès group [82] and displayed in figure 9(j), is a macroscopic tuning fork [112] based approach that can be used to probe the mechanical impedance, Z^*, of a confined system. By controlling both the normal and shear oscillations, the contributions from the stiffness of the system, Z', and dissipative loss in the system, Z'', can be determined. It makes use of principles and techniques common in atomic force microscopy to extend the capabilities

of the SFA, whilst also using a stiff piezoscanner [112] to define an absolute distance. The MiMes therefore overcomes the limitations of both of these common surface-probing techniques and was successful in characterising the molecular layering of the ionic liquid, [BMIM][PF_4]. [82] As distance can be absolutely defined without the need for white light interferometry, there is great versatility in the range of systems and surfaces that can be studied and the relationship between Z'' and viscosity accommodates the sensitive probing of hydrodynamical behaviour.

3.3. Measurement of shear forces, friction and energy dissipation

Dynamic and frictional properties of confined films have been studied using the SFB over many years. [113, 43, 63, 65, 66, 72]. One fundamental question of longstanding interest concerns the mechanism of 'stick-slip' friction; the alternating catching and shearing of surfaces which is known to occur from the macroscopic scale (e.g. earthquakes) down to molecular scales[114, 115]. Many experiments and simulations have contributed towards building an understanding of this process, which appeared to involve sequential freezing-melting or freezing-shearing cycles in molecular films. A recent experimental study concluded that no melting transition occurs in the film during the periods of surface shear, and so the mechanism more likely involves inter-layer slips. [116] A particularly high-resolution instrument was designed by Klein and Kumacheva to detect the lateral coupling across layers with largely fluidic properties [58, 71]. Originally designed to measure the ultra-weak shear coupling across lubricious polymer brushes, the SFB design of Klein and Kumacheva applies the shearing motion using a piezoelectric tube (PZT), and determines the shear forces via an air-gap capacitor. [58] By applying voltage in different combinations to different parts of the sectored PZT, a diverse range of motion of one surface relative to the other can be achieved. Simultaneous and angstrom-scale motion in the vertical and lateral directions allows for concurrent measurement of film thickness, normal load, and friction force[59]; see figure 13.

Surface force balances optimised in this way, able to measure shear coupling with fine resolution, have been used to investigate the molecular mechanisms of friction in a wide variety of scenarios involving molecular fluids[32, 29], polymers[30], ionic liquids[119, 120, 118], and biological lipid membranes[31]. For example, the details of lubrication occurring in synovial joints has been of particular focus, with the insights gained feeding in to the design of artificial joints and other therapeutic treatments. The insight that water bound to charged headgroups of the lipids and saccharides can act as a molecular-scale lubricant has been termed *hydration lubrication*[121].

As always in the study of friction, a fundamental question concerns the mechanism of energy dissipation. In a study by Klein, the response signal from the spring motion during stick-slip sliding across a simple organic fluid was analysed to show that most of the energy is dissipated as viscous heating during the slip phase. The remaining energy is dissipated mechanically at the sticking/solidification point, evidenced by decaying oscillations in the deflection-time trace.[122] Insights of this sort are fundamental to the

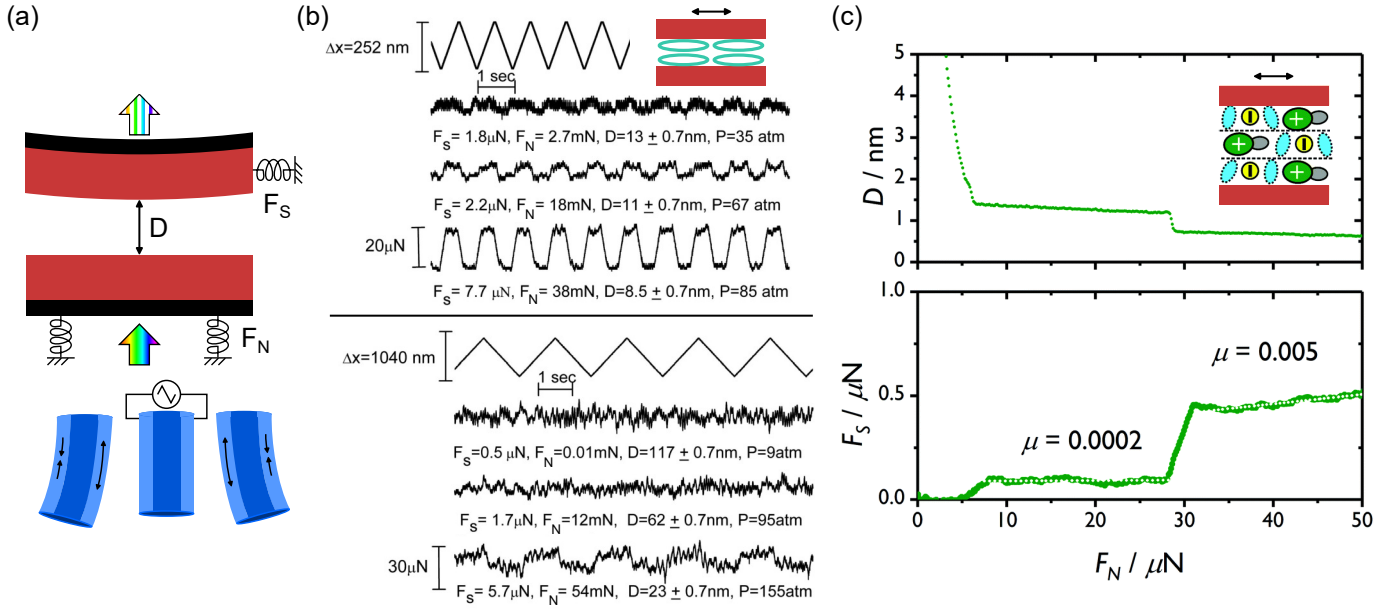

Figure 13. The shear force SFB and example measurements. (a): Schematic of the shear force SFB design of Klein and Kumacheva [58]. The upper mica surface is glued to a lens mounted on a sectored piezoelectric tube. Applying equal and opposite voltages to opposite sectors of the tube result in lateral motion. Surface separation D and normal forces F_N are measured by white light interferometry and by monitoring the deflection of a normal spring, while shear forces F_s may be measured by the deflection of a shear spring perpendicular to the passage of light. (b): Shear forces measured across thin films of small unilamellar vesicles (SUVs). Results from SUVs of DPPC (*above*) and DSPC (*below*) are shown, with the applied lateral motion shown above and shear forces shown below at increasing pressures. DSPC films are seen to have greater lubricating properties at higher pressures. Reprinted with permission from R. Sorkin, N. Kampf, Y. Dror, E. Shimoni, and J. Klein, *Biomaterials*, 34, 22, 5465-5475 [117]. (c): Simultaneous measurement of normal and shear forces across a thin film of the deep eutectic solvent ethaline in dry conditions. The measured friction coefficient of the film is 'quantised', showing unique values that depend on the number of molecular layers in the confined film. Reprinted with permission from J. E. Hallett, H. J. Hayler, and S. Perkin, *Physical Chemistry Chemical Physics*, 22, 20253-20264 [118].

understanding of energy dissipation in mechanical systems.

3.4. Measuring contact mechanics and soft-solid deformations

Understanding contact mechanics and the surface deformation of soft-solid surfaces is key in biological systems, tribology, and rheology. In biological environments, adhesion is achieved within aqueous surroundings and the study of this 'wet adhesion' has been particularly rich for its promise of useful biomimetic technologies. For example, the adhesion of marine molluscs to rock surfaces has been attributed to coordination between delocalised pi-systems and strongly cationic peptides; these mechanisms and details have been interrogated using the SFA in Israelachvili's group.[123, 124, 125] Wang *et al.* have used the SFA to study the deformation of a compliant surface in place of the usual

rigid mica surfaces. [126] In their setup one surface is rigid whilst the other is a soft polydimethylsiloxane (PDMS) film. Across a silicone oil, they study the deformation of the PDMS film on approaching the two surfaces using white light multiple-beam interferometry (figure 14). They showed that as the surfaces approach, the changing shape of the FECO interference pattern could be used to track the deformation of the softer surface as a result of hydrodynamic forces. Under some conditions a dimple was observed at the point of closest approach indicating a pocket of oil confined at the centre point.

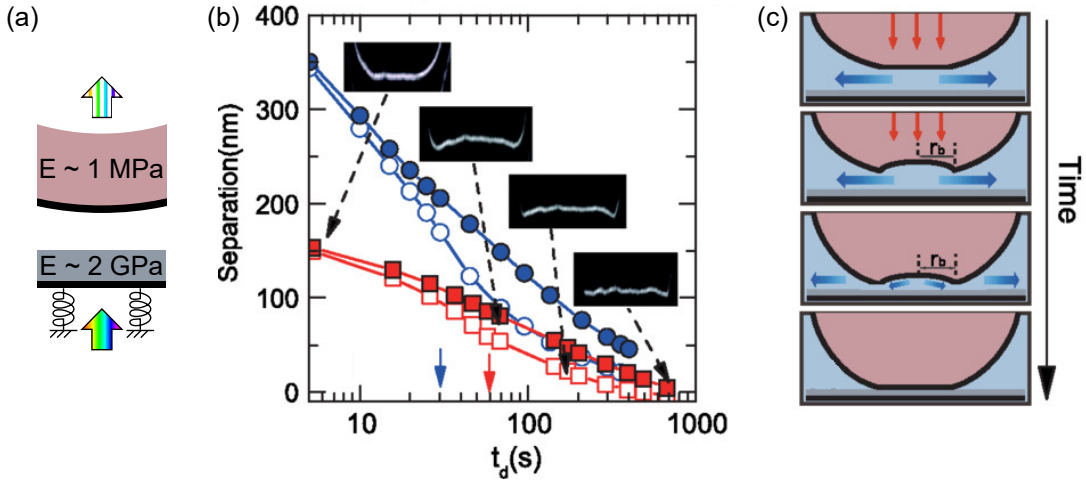

Figure 14. The soft-solid SFA and an example measurement. (a): Schematic of the soft-solid SFA. The upper lens is coated in a layer of polydimethyl siloxane (PDMS), with a Young's modulus $E \sim 1$ MPa, while the lower lens is coated in a material with $E \sim 2$ GPa. Thus the upper surface is highly deformable while the lower lens is effectively rigid. Approaching the surfaces rapidly in a viscous fluid can lead to flattening and the formation of a 'dimple' in the upper surface as it deforms. Surface separation and upper surface geometry are measured by white light interferometry, while normal forces can be measured by monitoring the deflection of a normal spring. (b): Surface separation as a function of time for two different drive velocities (blue circles and red squares), comparing the centre of the upper surface (filled symbols) and the edge of the upper surface (open symbols). When the edge of the upper surface is closer to the lower surface than the centre, a dimple may be said to have formed. (c): Schematic showing formation and relaxation of the dimples. Reprinted figures with permission from Y. Wang, C. Dhong, and J. Frechette, *Physical Review Letters*, 115, 248302, 2015. Copyright 2015 by the American Physical Society. [126]

3.5. Simultaneous determination of surface forces with in-plane fluid structure

3.5.1. X-Ray SFA. The SFA measures with extremely fine resolution (in distance and force) a statistical average interactions between surfaces across fluids. Implicitly, analysis of the SFB data often draws on the ergodic hypothesis to infer space-average structure from a time-averaged measurement of interaction free energy. However, in some cases this interpretation does not hold; in particular when the structure of the

material in the soft or fluid film is not laterally homogeneous. For this purpose the X-ray surface forces apparatus (X-SFA) was devised, to combine force-distance and X-ray scattering measurements. These complementary techniques allow controlled confinement of the sample with the ability to directly probe the confined structure using x-ray scattering or reflectometry. With this in mind, several versions of the X-SFA [127, 128, 129, 130] and other X-ray [131, 132, 133] and neutron [134, 135, 136] beam techniques have been used to study confined liquids. While these pioneering instruments were able to confine fluids to films of the order of 100's nm and made many interesting observations at that scale, it still remained desirable to investigate the lateral structure of films closer to molecular dimensions. This was achieved in an apparatus by Kekicheff, which was able to measure lateral structure in an inhomogeneous film at the same time as recording the film thickness with nanometric precision at distances less than 10nm. [137] With this apparatus it was possible to observe the simultaneous structural changes in surfactant aggregates during confinement down to nanoscopic dimensions; an effect attributed to the redistribution of counterions. This result contributed to an earlier interesting discussion of the interaction between net-neutral surfaces coated inhomogeneously with positive and negative patches[138, 139]. Initially, the unexpected observation that attractive forces act between 'charge mosaic' surfaces was thought to arise from rearrangement and correlation of the surface structure during approach. Later, it was also discovered that an attractive force is predicted for such neutral-heterogeneous surfaces within the Poisson-Boltzmann attraction due to an asymmetry between repulsive and attractive electrostatic forces in a screening environment.[139]

After this, Mezger *et al.* [84] recognised the need for a X-SFA that would allow dynamic measurements to be made. Their design uses a cylinder-on-flat geometry (see figure 9(l)) that confines a greater sample volume compared with the curved geometry setup. This makes dynamic in-plane scattering and specular X-ray reflectivity (XRR) measurements feasible. The geometry allows for the structure to be studied both parallel and perpendicular to the confining surfaces. Normal and lateral motion of the confining surfaces can be applied to measure normal and frictional forces, whilst simultaneously monitoring the structural changes *in situ*. Static measurements at a known and well-controlled surface separation are also possible with this instrument. This X-SFA has been used to study the structure of a model liquid crystal system under static and dynamic conditions. [84] They confined the liquid crystal (8CB) to a fixed gap width, applied a compression-decompression sequence and measured the specular XRR and in-plane scattering intensities. In micron-sized gaps, the compression and decompression strongly affects the orientational order of the liquid crystal. The relaxation process is also eight orders of magnitude slower than the bulk molecular relaxation time. No relaxation process is observed for a smaller gap width of 120 nm, suggesting defects are trapped on this timescale.

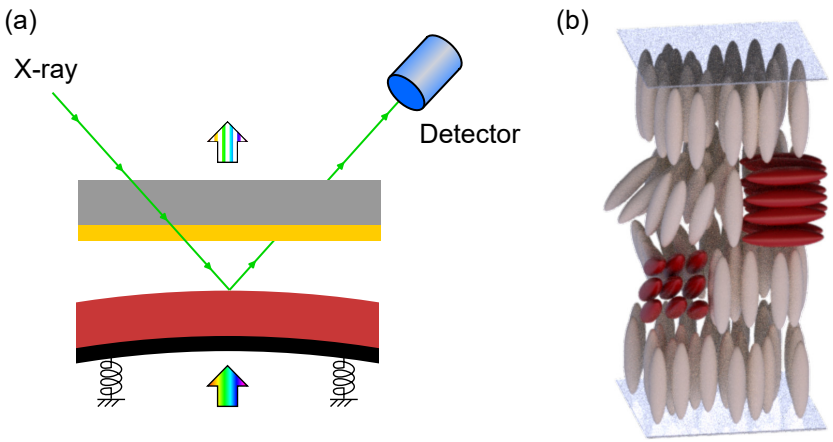

Figure 15. The X-SFA and example results. (a): Schematic of the X-SFA. The lower surface is a cylindrical, back silvered mica sheet, similar to other SFB/SFA set ups. The upper surface is template stripped gold on a flat, single crystal of corundum. The cylinder-on-flat geometry gives rise to a long, narrow contact region rather than a single spot. X-ray radiation may be shone along the direction of the cylinder apex, avoiding scattering artefacts from the mica edges. The X-ray beams must pass through several millimetres of the corundum crystal, so high energy X-rays are necessary. The lower surface may be raised, lowered, or sheared as required by the experiment. Surface separation is measured by white light interferometry and normal and lateral forces can be measured by strain gauges. (b): Sketch of the molecular structure of the confined liquid crystal 8CB, based on measurements made in the X-SFA. Aligned and misaligned domains are shown in brown and red respectively. The solid surfaces (blue) induce an orientation with the liquid crystal director perpendicular to the face of the surfaces. As the surfaces are brought together, misaligned domains can be distorted if their director points in the direction of flow. The overall structure of the liquid crystal hence becomes more aligned on confinement as the aligned domains remain intact during compression. Reproduced from reference [84].

4. New directions and outlook

The SFB, and its many versions, remains relevant as the scientific challenges ahead of us evolve. Many open questions arising in the fields of energy storage, environmental science, materials discovery, and bio-medical science require detailed analysis of interfacial structure, interactions and dynamics. Beyond these application directions, the SFB may help us as we interrogate new classes of matter and new light-matter interactions. Despite the difficulty of making predictions, especially about the future, we present some imaginings of these lines of enquiry.

Dynamical properties of electrode-electrolyte interfaces. As our energy revolution progresses it becomes increasingly important that new electrochemical energy storage materials (electrodes and electrolytes) are designed to be fully recyclable and of lower environmental impact. Technological advances in this area require detailed knowledge of the molecular and electronic processes occurring at the electrode-electrolyte interface, including liquid and soft electrolytic materials. Buried interfaces, such as the electrode-electrolyte interface inside a battery or supercapacitor, are challenging to characterise

at the molecular level in any case. However, additional difficulties arise when the interface is dynamic; it is important to understand the fast rearrangements of ions and solvent as the electrode voltage is switched, and irreversible chemical changes during cycling that lead to solid electrolyte interphase (SEI) formation. The SFB can provide high resolution measurements and insights in this regard, as hinted by recent proof-of-concept measurement by Tivony *et al.*: the charging dynamics of an electrode-electrolyte interface in confined geometry was determined from the measured force, revealing the timescale of electrical double layer relaxation after voltage switching at the electrode interface. Furthermore, new apparatus such as that described by Valtiner's research team will enable discoveries in this direction[140], and their initial studies have already begun to image the growth of electrode SEI layers in situ during cycling.[141] Future work in this direction might involve analysis of electrochemical systems involving faradic and capacitive energy storage, so-called pseudo-capacitors, as well as polymer and poly-ionic liquid electrolytes. By detecting the charge transferred between the mirror-electrodes at the same time as switching applied voltage, the double layer capacitance and charging time can be determined for electrode pore sizes down to nanometric scales. But indeed, it is not only the electrodes and interfaces which present a challenge to our understanding in this area; the highly concentrated electrolytes present in batteries are beyond the realm of dilute solution theories and remain challenging for computer modelling. Experiments are needed to further understand the electrical double layer in highly concentrated electrolytes.[142, 143] In general, we have the principle that electrochemical processes can be studied from deep inside the electrical double layer.

Iontronics and the dynamics of water and ions at the angstrom scale. As the design and fabrication of porous materials for energy and environmental applications such as filtration and osmotic energy generation reaches nanometric and sub-nanometic dimensions, we meet the need to understand more deeply the dynamic properties of water and electrolytes in these extreme degrees of confinement. The subtle details of wall-electrolyte interactions and ion hydration in nanoconfinement can lead to dramatic effects [144, 145, 146, 147, 148, 149, 150]. Inspired by biological mechanisms of signalling, energy storage and transfer, the new field of *iontronics* was born, as a versatile and energy-efficient soft alternative to electronics. In the mindset of Lydéric Bocquet: extraordinary possibilities lie ahead if we exchange the "grey" electrons for "ions with taste and colours"[151, 152]. To progress the field of iontronics, the most subtle of ionic effects must be properly disentangled. The SFB should help us step up to this challenge, to assist in resolving properties of dielectrics, solvation, field effects in confinement, chemical gradient effects, interfacial slippage, dehydration and transport of solvated ions and ionic materials at the angstrom scale.[153, 110, 36, 54, 73]

Deposition and erosion at solid interfaces in situ. Another frontier in understanding surface forces involves the effect of chemical gradients and phase transitions, such as erosion and weathering, on surface interactions. Adapting the SFB for the study of rough mineral and metallic materials has begun to open the way for study of such processes *in situ*, allowing for visualisation of the contact geometry and confined fluid

properties. In this direction, several research teams have been active in studying the forces involved in erosion, salt deposition, and other dynamic processes involved in interfacial aging by salts in aqueous environments[154, 97, 155, 156]. The great strength of SFB in this direction is the facility for direct visualisation of the interface, through the FECO interference pattern, at the same time as interaction force measurements which can reveal changes to adhesion, liquid film thickness and structure, fluidity, etc. Particularly active in this area recently has been the research teams of Dziadkowiec and Røyne, and of Espinoza-Marzal[157, 156, 158, 159]. Studies of the mineralisation of calcite in confined geometry[157, 156] revealed surprisingly long-ranged forces related to ion aggregation before mineral deposits are formed. Confined geometry can also bring about pressure solution, i.e. chemomechanical forces that lead to dissolution [158, 159]. The delicate and non-equilbrium processes involved in mineral formation in marine environments will draw substantial focus in the coming decades as efforts to nudge the carbon cycle in favour of sequestration become more urgent; studies such as these show how the SFB is well placed to reveal molecular details and insights into the mechanisms involved.

Interactions involving dynamic bio-interfaces. Within and between eukaryotic cells, a multitude of reactions and processes occur in highly confined environments and at interfaces. In traditional biochemical and biophysical studies, systems are studied either in solution or confined to a single interface (such as a glass coverslip). Yet, in many cases, proximity of two interfaces, or confinement itself, is a driving force. In these cases the SFB can be a useful tool for measuring the interaction arising when two biomaterials or biomolecular layers approach or recede from contact, or for creating controlled confinement geometry for a system of interest. SFB experiments have already demonstrated many examples of lipid bilayer interactions, e.g. bilayer fusion, hydration lubrication involving glycans and lipids. But nature is complex and much lies ahead. For example: (i) the recent demonstration that extracellular fluid viscosity enhances cell migration should inspire experiments to unpick the forces at play in such systems[160]; (ii) the heterogeneous nature of membranes with raft regions providing solubilising environments for hydrophobic proteins inspires questions about membrane-membrane interactions between raft-containing leaflets[161].

Quantum optics. In a dramatic departure from the classical systems studied using similar apparatus until this point, it has recently been pointed out that the SFB can be used as an ideal resonator for the study of quantum optical effects. In Zappone's lab, the SFB was set up as a metal-dielectric-metal resonator with cavity thicknesses ranging from micrometers down to nanometres for the direct study of polaritons generated in the cavity.[162] The crossed-cylinder geometry leads to continuous variation in resonator thickness in a single measurement; the SFB presents, essentially, an advanced and customisable Fabry-Perot interferometer for direct access to many parameters relevant to the study and design of quantum optical materials such as 'epsilon near zero' (ENZ) materials. [162, 163]. Analogues of molecular hybridisation – energy quantization, bonding and antibonding orbitals, avoided crossings

– are observed in macroscopic resonant cavities. It seems that this relatively simple lab-based experiment can illuminate mysteries of quantum mechanics and bonding using white light interferometry!

Fluids out of equilibrium and active matter. The statistical mechanics of systems far from equilibrium remains a theoretical topic in its infancy, and one of the most hotly discussed recent topics within this domain is active matter.[164] *Active* systems are those which continuously convert stored energy (e.g. chemical energy) into motion of the constituent units. This principle applies across many scales, e.g. microscale colloidal particles or bacteria, up to whole animal swarms, shoals, or flocks. Many curious observations and calculations of the properties of active systems test our intuition and remind us of the limited reach of equilibrium statistical mechanics. For example, active matter can contain non-reciprocal interactions; interactions can cause motion to be strongly correlated; and indeed pressure is not a well defined state function in active systems. Force generation and pressure are central concepts in active systems. What do we expect for the disjoining pressure, as measurable in the SFB, for a system of self-propelled particles? How does the rate of force generation and density of particles relate to the measured pressure in the system? What would we expect for the lateral (shear) forces transmitted across an active system? Could we observe phase transitions induced by confinement?

Over more than 50 years, measurements using the SFB have led to important insights and fundamental understanding of molecular interactions, fluids in confinement, and surface forces. This breadth of study has been made possible by the great versatility of the SFB as a tool for the molecular sciences. Many fundamental issues of molecular and surface forces arise in fields as diverse as electrochemical energy storage and conversion, environmental remediation, carbon sequestration, and biomedical sciences; the SFB will assist as we address these and many other scientific challenges of the future.

Acknowledgements

The authors would like to extend thanks to the students and postdocs who have contributed over many years towards the effort to optimise and develop the surface force balances in our research group in London then in Oxford. In particular, thanks to Nico Cousens, Florian Hausen, Marco Balabajew, Romain Lhermerout, Carla Perez-Martinez, James Hallett, Alex Smith, and Christian van Engers. The authors were supported in this work by The Leverhulme Trust (RPG-2015-328 and Philip Leverhulme Prize) and the European Research Council (under Starting Grant No. 676861, LIQUISWITCH, and Consolidator Grant No. 101001346, ELECTROLYTE). TG is grateful to the Worcester College Taylor Scholarship.

Open Access: This research was funded in whole or in part by the European Research Council, grant number 101001346. For the purpose of Open Access, the author has applied a CC BY public copyright licence to any Author Accepted Manuscript

(AAM) version arising from this submission.

[1] Jean Comtet, Guillaume Chatté, Antoine Niguès, Lydéric Bocquet, Alessandro Siria, and Annie Colin. Pairwise frictional profile between particles determines discontinuous shear thickening transition in non-colloidal suspensions. *Nature Communications*, 8:15633, 2017.

[2] David Labonte and Walter Federle. Rate-dependence of 'wet' biological adhesives and the function of the pad secretion in insects. *Soft Matter*, 11:8661–8673, 2015.

[3] Patrice Simon and Yury Gogotsi. Perspectives for electrochemical capacitors and related devices. *Nature Materials*, 19:1151–1163, 2020.

[4] Anke Weidenkaff, Ronja Wagner-Wenz, and Angelika Veziridis. A world without electronic waste. *Nature Reviews Materials*, 6:462–463, 2021.

[5] Aron Stubbins, Kara Lavender Law, Samuel E. Muñoz, Thomas S. Bianchi, and Lixin Zhu. Plastics in the earth system. *Science*, 373:51–55, 2021.

[6] Matthew Macleod, Hans Peter H. Arp, Mine B. Tekman, and Annika Jahnke. The global threat from plastic pollution. *Science*, 373:61–65, 2021.

[7] Dóra Takács, Tamás Szabó, Andrej Jamnik, Matija Tomšič, and István Szilágyi. Colloidal interactions of microplastic particles with anionic clays in electrolyte solutions. *Langmuir*, 39(36):12835–12844, 09 2023.

[8] J. N. Israelachvili and D Tabor. Measurement of van der waals dispersion forces in the range 1.4 to 130 nm. *Nature Physical Science*, 236:106, 1972.

[9] J. N. Munday, Federico Capasso, and V. Adrian Parsegian. Measured long-range repulsive casimir–lifshitz forces. *Nature*, 457:170–173, 2009.

[10] Paul F. Luckham and Jacob Klein. Interactions between smooth solid surfaces in solutions of adsorbing and nonadsorbing polymers in good solvent conditions. *Macromolecules*, 18:721–728, 1985.

[11] Alexander M. Smith, Michal Borkovec, and Gregor Trefalt. Forces between solid surfaces in aqueous electrolyte solutions. *Advances in Colloid and Interface Science*, 275:102078, 2020.

[12] Yan Levin. Electrostatic correlations: from plasma to biology. *Reports on Progress in Physics*, 65:1577–1632, 2002.

[13] P. Nelson. *Biological Physics: Energy, Information, Life*. WH Freeman, 2007.

[14] Salman F. Banani, Hyun O. Lee, Anthony A. Hyman, and Michael K. Rosen. Biomolecular condensates: organizers of cellular biochemistry. *Nature Reviews Molecular Cell Biology*, 18(5):285–298, 2017.

[15] Jacob Israelachvili. *Intermolecular and Surface Forces*. Elsevier, 2011.

[16] Ian M. Hutchings. Leonardo da vinci's studies of friction. *Wear*, 360–361:51–66, 2016.

[17] B. V. Derjaguin, A. S. Titijevskaia, I. I. Abricossova, and A. D. Malkina. Investigations of the forces of interaction of surfaces in different media and their application to the problem of colloid stability. *Discussions of the Faraday Society*, 18:24–41, 1954.

[18] J. Th. G. Overbeek and M. J. Sparnaay. Experiments on long-range attractive forces between macroscopic objects. *Journal of Colloid Science*, 7:343–345, 1952.

[19] Anita I. Bailey and J. S. Courtney-Pratt. The area of real contact and the shear strength of monomolecular layers of a boundary lubricant. *Proceedings of the Royal Society of London. Series A. Mathematical and Physical Sciences*, 227:500–515, 1955.

[20] D. Tabor and R. H. S. Winterton. Surface forces: direct measurement of normal and retarded van der waals forces. *Nature*, 219:1120–1121, 1968.

[21] Jacob N. Israelachvili and Gayle E. Adams. Measurement of forces between two mica surfaces in aqueous electrolyte solutions in the range 0–100 nm. *J. Chem. Soc., Faraday Trans. 1*, 74:975–1001, 1978.

[22] J. Israelachvili, Y. Min, M. Akbulut, A. Alig, G. Carver, W. Greene, K. Kristiansen, E. Meyer, N. Pesika, K. Rosenberg, and H. Zeng. Recent advances in the surface forces apparatus (SFA) technique. *Rep. Prog. Phys.*, 73:036601, 2010.

[23] Jacob Klein. Forces between mica surfaces bearing adsorbed macromolecules in liquid media. *J. Chem. Soc., Faraday Trans. 1*, 79:99–118, 1983.

[24] Georges. Hadziioannou, Sanjay. Patel, Steve. Granick, and Matthew. Tirrell. Forces between surfaces of block copolymers adsorbed on mica. *Journal of the American Chemical Society*, 108(11):2869–2876, 05 1986.

[25] Weifeng Lin and Jacob Klein. Direct measurement of surface forces: Recent advances and insights. *Applied Physics Reviews*, 8(3):031316, 09 2021.

[26] J. N. Israelachvili and G. E. Adams. Direct measurement of long range forces between two mica surfaces in aqueous kno$_3$ solutions. *Nature*, 262:774–776, 1976.

[27] Jacob Israelachvili and Richard Pashley. The hydrophobic interaction is long range, decaying exponentially with distance. *Nature*, 300:341–342, 1982.

[28] Michael Urbakh, Joseph Klafter, Delphine Gourdon, and Jacob Israelachvili. The nonlinear nature of friction. *Nature*, 430:525–528, 2004.

[29] Alexander M. Smith, James E. Hallett, and Susan Perkin. Solidification and superlubricity with molecular alkane films. *Proceedings of the National Academy of Sciences*, 116:25418–25423, 2019.

[30] Uri Raviv, Suzanne Giasson, Nir Kampf, Jean-François Gohy, Robert Jérôme, and Jacob Klein. Lubrication by charged polymers. *Nature*, 425:163–165, 2003.

[31] Wuge H. Briscoe, Simon Titmuss, Fredrik Tiberg, Robert K. Thomas, Duncan J. McGillivray, and Jacob Klein. Boundary lubrication under water. *Nature*, 444:191–194, 2006.

[32] Uri Raviv, Pierre Laurat, and Jacob Klein. Fluidity of water confined to subnanometre films. *Nature*, 413:51–54, 2001.

[33] Romain Lhermerout and Susan Perkin. Nanoconfined ionic liquids: Disentangling electrostatic and viscous forces. *Phys. Rev. Fluids*, 3:014201, 2018.

[34] Let's talk about lipid nanoparticles. *Nature Reviews Materials*, 6:99, 2021.

[35] Z. Lin, E. Goikolea, A. Balducci, K. Naoi, P. L. Taberna, M. Salanne, G. Yushin, and P. Simon. Materials for supercapacitors: when li-ion battery power is not enough. *Materials Today*, 21:419–436, 2018.

[36] Fernando Bresme, Alexei A. Kornyshev, Susan Perkin, and Michael Urbakh. Electrotunable friction with ionic liquid lubricants. *Nature Materials*, 21:848–858, 2022.

[37] S. Tolansky. *Multiple-beam interferometry of surfaces and films*. Oxford University Press, 1948.

[38] J. N. Israelachvili. Thin film studies using multiple-beam interferometry. *Journal of Colloid and Interface Science*, 44:259–272, 1973.

[39] Hugo K. Christenson and Neil H. Thomson. The nature of the air-cleaved mica surface. *Surface Science Reports*, 71:367–390, 2016.

[40] Jacob N. Israelachvili, Norma A. Alcantar, Nobuo Maeda, Thomas E. Mates, and Marina Ruths. Preparing contamination-free mica substrates for surface characterization, force measurements, and imaging. *Langmuir*, 20:3616–3622, 2004.

[41] Susan Perkin, Liraz Chai, Nir Kampf, Uri Raviv, Wuge Briscoe, Iain Dunlop, Simon Titmuss, Minseok Seo, Eugenia Kumacheva, and Jacob Klein. Forces between mica surfaces, prepared in different ways, across aqueous and nonaqueous liquids confined to molecularly thin films. *Langmuir*, 22:6142–6152, 2006.

[42] Alex M. Schrader, Jacob I. Monroe, Ryan Sheil, Howard A. Dobbs, Timothy J. Keller, Yuanxin Li, Sheetal Jain, M. Scott Shell, Jacob N. Israelachvili, and Songi Han. Surface chemical heterogeneity modulates silica surface hydration. *Proceedings of the National Academy of Sciences*, 115(12):2890–2895, 2018.

[43] Joanna Janik, Rafael Tadmor, and Jacob Klein. Shear of molecularly confined liquids crystals. 1. orientation and transitions under confinement. *Langmuir*, 13:4466–4473, 1997.

[44] Dominika Nowak, Manfred Heuberger, Michael Zäch, and Hugo K. Christenson. Thermodynamic and kinetic supercooling of liquid in a wedge pore. *The Journal of Chemical Physics*, 129:154509, 2008.

[45] Dominika Nowak and Hugo K. Christenson. Capillary condensation of water between mica surfaces above and below zero-effect of surface ions. *Langmuir*, 25:9908–9912, 2009.

[46] Hugo K. Christenson. Phase behavior in confinement studied with a surface force apparatus. *Journal of Dispersion Science and Technology*, 27:617–624, 2006.

[47] Alexander Artsyukhovich, Leonard D. Broekman, and Miquel Salmeron. Friction of the liquid crystal 8cb as probed by the surface forces apparatus. *Langmuir*, 15:2217–2223, 1999.

[48] Marina Ruths and Bruno Zappone. Direct nanomechanical measurement of an anchoring transition in a nematic liquid crystal subject to hybrid anchoring conditions. *Langmuir*, 28:8371–8383, 2012.

[49] Kai Kristiansen, Hongbo Zeng, Bruno Zappone, and Jacob N. Israelachvili. Simultaneous measurements of molecular forces and electro-optical properties of a confined 5cb liquid crystal film using a surface forces apparatus. *Langmuir*, 31:3965–3972, 2015.

[50] Bruno Zappone, Weichao Zheng, and Susan Perkin. Multiple-beam optical interferometry of anisotropic soft materials nanoconfined with the surface force apparatus. *Review of Scientific Instruments*, 89:085112, 2018.

[51] Weichao Zheng, Carla Sofia Perez-Martinez, Gia Petriashvili, Susan Perkin, and Bruno Zappone. Direct measurements of structural forces and twist transitions in cholesteric liquid crustal films with surface force apparatus. *Soft Matter*, 15:4905–4914, 2019.

[52] Bruno Zappone and Roberto Bartolino. Topological barriers to defect nucleation generate large mechanical forces in an ordered fluid. *Proceedings of the National Academy of Sciences*, 118:e2110503118, 2021.

[53] Uri Raviv, Joseph Frey, Rinat Sak, Pierre Laurat, Rafael Tadmor, and Jacob Klein. Properties and interactions of physigrafted end-functionalized poly(ethylene glycol) layers. *Langmuir*, 18:7482–7495, 2002.

[54] Di Jin, Yongyun Hwang, Liraz Chai, Nir Kampf, and Jacob Klein. Direct measurement of the viscoelectric effect in water. *Proceedings of the National Academy of Sciences*, 119:e2113690119, 2022.

[55] Uri Raviv, Susan Perkin, Pierre Laurat, and Jacob Klein. Fluidity of water confined down to subnanometer films. *Langmuir*, 20(13):5322–5332, 2004. PMID: 15986669.

[56] Alexander M. Smith, Alpha A. Lee, and Susan Perkin. Switching the structural force in ionic liquid-solvent mixtures by varying composition. *Physical Review Letters*, 118:096002, 2017.

[57] Hisae Yoshizawa, You Lung Chen, and Jacob Israelachvili. Fundamental mechanisms of interfacial friction. 1. relation between adhesion and friction. *The Journal of Physical Chemistry*, 97(16):4128–4140, 04 1993.

[58] Jacob Klein and Eugenia Kumacheva. Simple liquids confined to molecularly thin layers. i. confinement-induced liquid-to-solid phase transitions. *The Journal of Chemical Physics*, 108:6996–7009, 1998.

[59] R. Lhermerout and S. Perkin. A new methodology for a detailed investigation of quantized friction in ionic liquids. *Phys. Chem. Phys. Chem.*, 22:455–466, 2020.

[60] D Tabor and R. H. S. Winterton. The direct measurement of normal and retarded van der waals forces. *Proc. Roy. Soc. A.*, 312:435–450, 1969.

[61] J. N. Israelachvili. Interferometric method for determining refractive index and thickness of thin films. *Nature Physical Science*, 229:85–86, 1971.

[62] J. N. Israelachvili and D Tabor. Shear properties of molecular films. *Nature Physical Science*, 241:148–149, 1973.

[63] J. N. Israelachvili and D Tabor. The shear properties of molecular films. *Wear*, 24:386–390, 1973.

[64] J. N. Israelachvili. Direct measurements of forces between surfaces in liquids at the molecular level. *Proc. Natl. Acad. Sci.*, 84:4722–4724, 1987.

[65] R. G. Horn and J. N. Israelachvili. Direct measurement of forces due to solvent structure. *Chem. Phys. Lett.*, 71:192–194, 1980.

[66] R. G. Horn and J. N. Israelachvili. Direct measurement of structural forces between two surfaces in a nonpolar liquid. *The Journal of Chemical Physics*, 75:1400–1411, 1981.

[67] M. Heuberger, G. Luengo, and J. N. Israelachvili. Topographic information from multiple beam interferometry in the surface forces apparatus. *Langmuir*, 13:3839–3848, 1997.

[68] M. Heuberger. The extended surface forces apparatus. part i. fast spectral correlation interferometry. *Rev. Sci. Instrum.*, 72:1700–1707, 2001.

[69] M. Heuberger, M. Zäch, and N. D. Spencer. Sources and control of instrumental drift in the surface forces apparatus. *Review of Scientific Instruments*, 71:4502–4508, 2000.

[70] Kai Kristiansen, Stephen H. Donaldson Jr., Zachariah J. Berkson, Jeffrey Scott, Rongxin Su, Xavier Banquy, Dong Woog Lee, Hilton B. de Anguiar, Joshua D. McGraw, George D. Degen, and Jacob N. Israelachvili. Multimodal miniature surface forces apparatus (μSFA) for interfacial science measurements. *Langmuir*, 35:15500–15514, 2019.

[71] Eugenia Kumacheva and Jacob Klein. Simple liquids confined to molecularly thin layers. ii. shear and frictional behavior of solidified films. *The Journal of Chemical Physics*, 108:7010–7022, 1998.

[72] Jacob N. Israelachvili and Richard M. Pashley. Molecular layering of water at surfaces and origin of repulsive hydration forces. *Nature*, 306:249–250, 1983.

[73] James E. Hallett, Kieran J. Agg, and Susan Perkin. Zwitterions fine-tune interactions in electrolyte solutions. *Proceedings of the National Academy of Sciences*, 120(8):e2215585120, 2023.

[74] Carlos Drummond. Electric-field-induced friction reduction and control. *Physical Review Letters*, 109:154302, 2012.

[75] Liraz Chai and Jacob Klein. Large area, molecularly smooth (0.2 nm rms) gold films for surface forces and other studies. *Langmuir*, 23:7777–7783, 2007.

[76] Carla Sofia Perez-Martinez and Susan Perkin. Surface forces generated by the action of electric fields across liquid films. *Soft Matter*, 15:4255–4265, 2019.

[77] Christian D. van Engers, Nico E. A. Cousens, Vitaliy Babenko, Jude Britton, Bruno Zappone, Nicole Grobert, and Susan Perkin. Direct measurement of the surface energy of graphene. *Nano. Lett.*, 17:3815–3821, 2017.

[78] Christian D. van Engers, Marco Balabajew, Astrid Southam, and Susan Perkin. A 3-mirror surface force balance for the investigation of fluids confined to nanoscale films between two ultra-smooth polarizable electrodes. *Review of Scientific Instruments*, 89:23901, 2018.

[79] Hiroshi Kawai, Hiroshi Sakuma, Masashi Mizukami, Takashi Abe, Yasuhiro Fukao, Haruo Tajima, and Kazue Kurihara. New surface forces apparatus using two-beam interferometry. *Rev. Sci. Instrum.*, 79:043701, 2008.

[80] F. Restagno, J. Crassous, E Charlaix, and M. Monchanin. A new capacitive sensor for displacement measurement in a surface-force apparatus. *Measurement Science and Technology*, 12:16–22, 2000.

[81] Frédéric Restagno, Jérôme Crassous, Élisabeth Charlaix, Cécile Cottin-Bizonne, and Michel Monchanin. A new surface forces apparatus for nanorheology. *Review of Scientific Instruments*, 73:2292–2297, 2002.

[82] Antoine Lainé, Laetitia Jubin, Luca Canale, Lydéric Bocquet, Alessandro Siria, Stephen H Donaldson Jr, and Antoine Niguès. Micromegascope based dynamic surface force apparatus. *Nanotechnology*, 30:195502, 2019.

[83] Jason N. Connor and Roger G. Horn. Measurement of aqueous film thickness between charged mercury and mica surfaces: A direct experimental probe of the poisson-boltzmann distribution. *Langmuir*, 17:7194–7197, 2001.

[84] Henning Weiss, Hsiu-Wei Cheng, Julian Mars, Hailong Li, Claudia Merola, Frank Uwe Renner, Veijo Honkimäki, Markus Valtiner, and Markus. Mezger. Structure and dynamics of confined liquids: Challenges and perspectives for the x-ray surface forces apparatus. *Langmuir*, 35:16679–16692, 2019.

[85] John M. Levins and T. Kyle Vanderlick. Impact of roughness of reflective films on the application of multiple beam interferometry. *J. Colloid Interface Sci.*, 158:223–227, 1993.

[86] John M Levins and T. Kyle Vanderlick. Impact of roughness on the deformation and adhesion of a rough metal and smooth mica in contact. *J. Phys. Chem.*, 99:5067–5076, 1995.

[87] John M. Levins and T. Kyle Vanderlick. Characterization of the interface between a rough metal and smooth mica in contact. *J. Colloid Interface Sci.*, 185:449–458, 1997.

[88] Martin Hegner, Peter Wagner, and Giorgio Semenza. Ultralarge atomically flat template-stripped gold surfaces for scanning probe microscopy. *Surf. Sci.*, 291:39–46, 1993.

[89] Peter Wagner, Martin Hegner, Hans Joachin Guntherodt, and Giorgio Semenza. Formation and in situ modification of monolayers chemisorbed on ultraflat template-stripped gold surfaces. *Langmuir*, 11:3867–3875, 1995.

[90] Ran Tivony, Dan Ben Yaakov, Gilad Silbert, and Jacob Klein. Direct observation of confinement-induced charge inversion at a metal surface. *Langmuir*, 31:12845–12849, 2015.

[91] Ran Tivony and Jacob Klein. Modifying surface forces through control of surface potentials. *Faraday Discussions*, 199:261–277, 2017.

[92] V. Adrian Parsegian and David Gingell. On the electrostatic interaction across a salt solution between two bodies bearing unequal charges. *Biophys. J.*, 12:1192–1204, 1972.

[93] Łukasz Richter, Paweł J. Żuk, Piotr Szymczak, Jan Paczesny, Krzysztof M. Bak, Tomasz Szymborski, Piotr Garstecki, Howard A. Stone, Robert Hołyst, and Carlos Drummond. Ions in an ac electric field: Strong long-range repulsion between oppositely charged surfaces. *Phys. Rev. Lett.*, 125:056001, Jul 2020.

[94] Jude Britton, Nico E. A. Cousens, Samuel W. Coles, Christian D. van Engers, Vitaliy Babenko, Adrian T. Murdock, Antal Koós, Susan Perkin, and Nicole Grobert. A graphene surface force balance. *Langmuir*, 30:11485–11492, 2014.

[95] Yongkang Wang, Yuki Nagata, and Mischa Bonn. Substrate effect on charging of electrified graphene/water interfaces. *Faraday Discuss.*, pages –, 2024.

[96] John M. Levins and T. Kyle Vanderlick. Extended spectral analysis of multiple beam interferometry: A technique to study metallic films in the surface forces apparatus. *Langmuir*, 10:2389–2394, 1994.

[97] Markus Valtiner, Xavier Banquy, Kai Kristiansen, George W. Greene, and Jacob N. Israelachvili. The electrochemical surface force apparatus: The effect of surface roughness, electrostatic surface potentials, and anodic oxide growth on interaction forces, and friction between dissimilar surfaces in aqueous solutions. *Langmuir*, 28:13080–13093, 2012.

[98] Motohiro Kasuya, Kazuhito Tomita, Masaya Hino, Masashi Mizukami, Hiroyuki Mori, Seiji Kajita, Toshihide Ohmori, Atsushi Suzuki, and Kazue Kurihara. Nanotribological characterization of lubricants between smooth iron surfaces. *Langmuir*, 33:3941–3948, 2017.

[99] Florian Lecadre, Motohiro Kasuya, Aya Harano, Yuji Kanno, and Kazue Kurihara. Low-temperature surface forces apparatus to determine the interactions between ice and silica surfaces. *Langmuir*, 34:11311–11315, 2018.

[100] Florian Lecadre, Motohiro Kasuya, Yuji Kanno, and Kazue Kurihara. Ice premelting layer studied by resonance shear measurement (rsm). *Langmuir*, 35:15729–15733, 2018.

[101] Sylvain Hemmette, Motohiro Kasuya, Florian Lecadre, Yuji Kanno, Denis Mazuyer, Juliette Cayer-Barrioz, and Kazue Kurihara. Viscoelasticity of rubber–ice interfaces under shear studied using low-temperature surface forces apparatus. *Tribol. Lett.*, 67:74, 2019.

[102] Toshio Kamijo, Motohiro Kasuya, Masashi Mizukami, and Kazue Kurihara. Direct observation of double layer interactions between the potential-controlled gold electrode surfaces using the electrochemical surface forces apparatus. *Chem. Lett.*, 40:674–675, 2011.

[103] Motohiro Kasuya, Tsukasa Sogawa, Takuya Masuda, Toshio Kamijo, Kohei Uosaki, and Kazue Kurihara. Anion adsorption on gold electrodes studied by electrochemical surface forces measurement. *J. Phys. Chem. C*, 120:15986–15992, 2016.

[104] Jason N. Connor and Roger G. Horn. Extending the surface force apparatus capabilities by using white light interferometry in reflection. *Review of Scientific Instruments*, 74:4601–4606, 2003.

[105] Léo Garcia, Chloé Barraud, Cyril Picard, Jérôme Giraud, Elisabeth Charlaix, and Benjamin

Cross. A micro-nano-rheometer for the mechanics of soft matter at interfaces. *Review of Scientific Instruments*, 87:113906, 2016.

[106] C. Cottin-Bizonne, S. Jurine, J. Baudry, J. Crassous, F. Restagno, and É. Charlaix. Nanorheology: An investigation of the boundary condition at hydrophobic and hydrophilic interfaces. *The European Physical Journal E*, 9:47–53, 2002.

[107] B. Cross, A. Steinberger, C. Cottin-Bizonne, J.-P. Rieu, and E. Charlaix. Boundary flow of water on supported phospholipid films. *Europhysics Letters*, 73:390–395, 2006.

[108] Audrey Steinberger, Cécile Cottin-Bizonne, Pascal Kleimann, and Elisabeth Charlaix. High friction on a bubble mattress. *Nature Materials*, 6:665–668, 2007.

[109] Richard Villey, Emmanuelle Martinot, Cécile Cottin-Bizonne, Magali Phaner-Goutorbe, Liliane Léger, Frédéric Restagno, and Elisabeth Charlaix. Effect of surface elasticity on the rheology of nanometric liquids. *Physical Review Letters*, 111:215701, 2013.

[110] Benjamin Cross, Chloé Barraud, Cyril Picard, Liliane Léger, Frédéric Restagno, and Élisabeth Charlaix. Wall slip of complex fluids: interfacial friction versus slip length. *Physical Review Fluids*, 3:062001, 2018.

[111] Chloé Barraud, Benjamin Cross, Cyril Picard, Fréderic Restagno, Lilianne Léger, and Elisabeth Charlaix. Large slippage and depletion layer at the polyelectrolyte/solid interface. *Soft Matter*, 15:6308–6317, 2019.

[112] Luca Canale, Axel Laborieux, Aroul. A. Mogane, Laetitia Jubin, Jean Comtet, Antoine Lainé, Lydéric Bocquet, Alessandro Siria, and Antoine Niguès. Micromegascope. *Nanotechnology*, 29:355501, 2018.

[113] J Israelachvili, Y Min, M Akbulut, A Alig, G Carver, W Greene, K Kristiansen, E Meyer, N Pesika, K Rosenberg, and H Zeng. Recent advances in the surface forces apparatus (sfa) technique. *Reports on Progress in Physics*, 73(3):036601, 2010.

[114] J. N. Israelachvili, P. M. McGuiggan, and A. M. Homola. Dynamic properties of molecularly thin liquid films. *Science*, 240:189–191, 1988.

[115] Michelle L. Gee, Patricia M McGuiggan, Jacob N. Israelachvili, and Andrew M. Homola. Liquid to solidlike transitions of molecularly thin films under shear. *The Journal of Chemical Physics*, 93:1895–1906, 1990.

[116] Irit Rosenhek-Goldian, Nir Kampf, Arie Yeredor, and Jacob Klein. On the question of whether lubricants fluidize in stick–slip friction. *Proceedings of the National Academy of Sciences*, 112(23):7117–7122, 2015.

[117] Raya Sorkin, Nir Kampf, Yael Dror, Eyal Shimoni, and Jacob Klein. Origins of extreme boundary lubrication by phosphatidylcholine liposomes. *Biomaterials*, 34(22):5465–5475, 2013.

[118] James E. Hallett, Hannah J. Hayler, and Susan Perkin. Nanolubrication in deep eutectic solvents. *Phys. Chem. Chem. Phys.*, 22:20253–20264, 2020.

[119] Alexander M. Smith, Michael A. Parkes, and Susan Perkin. Molecular friction mechanisms across nanofilms of a bilayer-forming ionic liquid. *Journal of Physical Chemistry Letters*, 5:4032–4037, 2014.

[120] Carla S. Perez-Martinez and Susan Perkin. Interfacial structure and boundary lubrication of a dicationic ionic liquid. *Langmuir*, 35(48):15444–15450, 12 2019.

[121] Liran Ma, Anastasia Gaisinskaya-Kipnis, Nir Kampf, and Jacob Klein. Origins of hydration lubrication. *Nature Communications*, 6(1):6060, 2015.

[122] Jacob Klein. Frictional dissipation in stick-slip sliding. *Physical Review Letters*, 98:056101, 2007.

[123] Greg P. Maier, Michael V. Rapp, J. Herbert Waite, Jacob N. Israelachvili, and Alison Butler. Adaptive synergy between catechol and lysine promotes wet adhesion by surface salt displacement. *Science*, 349(6248):628–632, 2015.

[124] Matthew A. Gebbie, Wei Wei, Alex M. Schrader, Thomas R. Cristiani, Howard A. Dobbs, Matthew Idso, Bradley F. Chmelka, J. Herbert Waite, and Jacob N. Israelachvili. Tuning underwater adhesion with cation–pi interactions. *Nature Chemistry*, 9(5):473–479, 2017.

[125] Emmanouela Filippidi, Thomas R. Cristiani, Claus D. Eisenbach, J. Herbert Waite, Jacob N.

Israelachvili, B. Kollbe Ahn, and Megan T. Valentine. Toughening elastomers using mussel-inspired iron-catechol complexes. *Science*, 358(6362):502–505, 2017.

[126] Yumo Wang, Charles Dhong, and Joelle Frechette. Out-of-contact elastohydrodynamic deformation due to lubrication forces. *Physical Review Letters*, 115:248302, 2015.

[127] Stefan H. J. Idziak, Cyrus R. Safinya, Robert S. Hill, Keith E. Kraiser, Marina Ruths, Heidi E. Warriner, Suzi Steinberg, Keng S. Liang, and Jacob N. Israelachvili. The x-ray surface forces apparatus: Structure of a thin smectic liquid crystal film under confinement. *Science*, 264:1915–1918, 1994.

[128] S. H. J. Idziak, I. Koltover, K. S. Liang, J. N. Israelachvili, and C. R. Safinya. Study of flow in a smectic liquid crystal in the x-ray surface forces apparatus. *Int. J. Thermophys.*, 16:299–307, 1995.

[129] Y. Golan, A. Martin-Herranz, Y. Li, C. R. Safinya, and J. Israelachvili. Direct observation of shear-induced orientational phase coexistence in a lyotropic system using a modified x-ray surface forces apparatus. *Phys. Rev. Lett.*, 86:1263–1266, 2001.

[130] Yuval Golan, Markus Seitz, Ci Luo, Ana Martin-Herranz, Mario Yasa, Youli Li, Cyrus R. Safinya, and Jacob Israelachvili. The x-ray surface forces apparatus for simultaneous x-ray diffraction and direct normal and lateral force measurements. *Review of Scientific Instruments*, 73:2486–2488, 2002.

[131] E. Perret, K. Nygård, D. K. Satapathy, T. E. Balmer, O. Bunk, M. Heuberger, and J. F. van der Veen. X-ray reflectivity reveals equilibrium density profile of molecular liquid under nanometre confinement. *EPL*, 88:36004, 2009.

[132] M. Lippmann, A. Ehnes, and O. H. Seeck. An x-ray setup to investigate the atomic order of confined liquids in slit geometry. *Rev. Sci. Instrum.*, 85:015106, 2014.

[133] Kazuhito Tomita, Masashi Mizukami, Shinya Nakano, Noboru Ohta, Naoto Yagi, and Kazue Kurihara. X-ray diffraction and resonance shear measurement of nano-confined ionic liquids. *Phys. Chem. Chem. Phys.*, 20:13714–13721, 2018.

[134] Tonya L. Kuhl, Gregory S. Smith, Jacob N. Israelachvili, Jaroslaw Majewski, and William Hamilton. Neutron confinement cell for investigating complex fluids. *Rev. Sci. Instrum.*, 72:1715–1720, 2001.

[135] Max Wolff, Philipp Gutfreund, Adrian Rühm, Bulent Akgun, and Hartmut Zabel. Nanoscale discontinuities at the boundary of flowing liquids: A look into structure. *J. Phys. Condens. Matter*, 23:184102–184111, 2011.

[136] M. Wolff, P. Kuhns, G. Liesche, J. F. Ankner, J. F. Browning, and P. Gutfreund. Combined neutron reflectometry and rheology. *J. Appl. Cryst.*, 46:1729–1733, 2013.

[137] P. Kékicheff, J. Iss, P. Fontaine, and A. Johner. Direct measurement of lateral correlations under controlled nanoconfinement. *Phys. Rev. Lett.*, 120:118001, Mar 2018.

[138] Susan Perkin, Nir Kampf, and Jacob Klein. Long-range attraction between charge-mosaic surfaces across water. *Phys. Rev. Lett.*, 96:038301, Jan 2006.

[139] Gilad Silbert, Dan Ben-Yaakov, Yael Dror, Susan Perkin, Nir Kampf, and Jacob Klein. Long-ranged attraction between disordered heterogeneous surfaces. *Phys. Rev. Lett.*, 109:168305, Oct 2012.

[140] Valentina Wieser, Pierluigi Bilotto, Ulrich Ramach, Hui Yuan, Kai Schwenzfeier, Hsiu-Wei Cheng, and Markus Valtiner. Novel in situ sensing surface forces apparatus for measuring gold versus gold, hydrophobic, and biophysical interactions. *Journal of Vacuum Science Technology A*, 39(2):023201, 01 2021.

[141] Boaz Moeremans, Hsiu-Wei Cheng, Claudia Merola, Qingyun Hu, Mehtap Oezaslan, Mohammadhosein Safari, Marlies K. Van Bael, An Hardy, Markus Valtiner, and Frank Uwe Renner. In situ mechanical analysis of the nanoscopic solid electrolyte interphase on anodes of li-ion batteries. *Advanced Science*, 6(16):1900190, 2019.

[142] Matthew A. Gebbie, Alexander M. Smith, Howard A. Dobbs, Alpha A. Lee, Gregory G. Warr, Xavier Banquy, Markus Valtiner, Mark W. Rutland, Jacob N. Israelachvili, Susan Perkin, and

Rob Atkin. Long range electrostatic forces in ionic liquids. *Chem. Commun.*, 53:1214–1224, 2017.

[143] Alexander M. Smith, Alpha A. Lee, and Susan Perkin. The Electrostatic Screening Length in Concentrated Electrolytes Increases with Concentration. *Journal of Physical Chemistry Letters*, 7(12):2157–2163, 2016.

[144] Alessandro Siria, Marie-Laure Bocquet, and Lydéric Bocquet. New avenues for the large-scale harvesting of blue energy. *Nature Reviews Chemistry*, 1(11):0091, 2017.

[145] Eleonora Secchi, Sophie Marbach, Antoine Niguès, Derek Stein, Alessandro Siria, and Lydéric Bocquet. Massive radius-dependent flow slippage in carbon nanotubes. *Nature*, 537(7619):210–213, 2016.

[146] Yi You, Abdulghani Ismail, Gwang-Hyeon Nam, Solleti Goutham, Ashok Keerthi, and Boya Radha. Angstrofluidics: Walking to the limit. *Annual Review of Materials Research*, 52:189–218, 2022.

[147] Ashok Keerthi, Solleti Goutham, Yi You, Pawin Iamprasertkun, Robert A. W. Dryfe, Andre K. Geim, and Boya Radha. Water friction in nanofluidic channels made from two-dimensional crystals. *Nature Communications*, 12:3092, 2021.

[148] Nikita Kavokine, Marie-Laure Bocquet, and Lydéric Bocquet. Fluctuation-induced quantum friction in nanoscale water flows. *Nature*, 602:84–90, 2022.

[149] Theo Emmerich, Kalangi S. Vasu, Ashok Niguès, Antoine Keerthi, Boya Radha, Alessandro Siria, and Lydéric Bocquet. Enhanced nanofluidic transport in activated carbon nanoconduits. *Nature Materials*, 21:696–702, 2022.

[150] Tianyi Han, Wei Cao, Zhi Xu, Vahid Adibnia, Matteo Olgiati, Markus Valtiner, Liran Ma, Chenhui Zhang, Ming Ma, Jianbin Luo, and Xavier Banquy. Hydration layer structure modulates superlubrication by trivalent la¡sup¿3+¡/sup¿ electrolytes. *Science Advances*, 9(28):eadf3902, 2023.

[151] Lydéric Bocquet. Concluding remarks: Iontronics, from fundamentals to ion-controlled devices – random access memories. *Faraday Discuss.*, 246:618–622, 2023.

[152] Yujia Zhang, Jorin Riexinger, Xingyun Yang, Ellina Mikhailova, Yongcheng Jin, Linna Zhou, and Hagan Bayley. A microscale soft ionic power source modulates neuronal network activity. *Nature*, 620(7976):1001–1006, 2023.

[153] Léo Garcia, Léa Jacquot, Elisabeth Charlaix, and Benjamin Cross. Nano-mechanics of ionic liquids at dielectric and metallic interfaces. *Faraday Discussions*, 206:443–457, 2018.

[154] Rosa M. Espinosa-Marzal and George W. Scherer. Advances in understanding damage by salt crystallization. *Accounts of Chemical Research*, 43(6):897–905, 06 2010.

[155] Buddha Ratna Shrestha, Qingyun Hu, Theodoros Baimpos, Kai Kristiansen, Jacob N. Israelachvili, and Markus Valtiner. Real-time monitoring of aluminium crevice corrosion and its inhibition by vandates with multiple beam interferometry in a surface forces apparatus. *Journal of The Electrochemical Society*, 162:C327–C332, 2015.

[156] Joanna Dziadkowiec, Shaghayegh Javadi, Jon E. Bratvold, Ola Nilsen, and Anja Røyne. Surface forces apparatus measurements of interactions between rough and reactive calcite surfaces. *Langmuir*, 34(25):7248–7263, 06 2018.

[157] Joanna Dziadkowiec, Bahareh Zareeipolgardani, Dag Kristian Dysthe, and Anja Røyne. Nucleation in confinement generates long-range repulsion between rough calcite surfaces. *Scientific Reports*, 9(1):8948, 2019.

[158] Yijue Diao, Anqi Li, and Rosa M. Espinosa-Marzal. Ion specific effects on the pressure solution of calcite single crystals. *Geochimica et Cosmochimica Acta*, 280:116–129, 2020.

[159] Binxin Fu, Yijue Diao, and Rosa M. Espinosa-Marzal. Nanoscale insight into the relation between pressure solution of calcite and interfacial friction. *Journal of Colloid and Interface Science*, 601:254–264, 2021.

[160] Kaustav Bera, Alexander Kiepas, Inês Godet, Yizeng Li, Pranav Mehta, Brent Ifemembi, Colin D. Paul, Anindya Sen, Selma A. Serra, Konstantin Stoletov, Jiaxiang Tao, Gabriel

Shatkin, Se Jong Lee, Yuqi Zhang, Adrianna Boen, Panagiotis Mistriotis, Daniele M. Gilkes, John D. Lewis, Chen-Ming Fan, Andrew P. Feinberg, Miguel A. Valverde, Sean X. Sun, and Konstantinos Konstantopoulos. Extracellular fluid viscosity enhances cell migration and cancer dissemination. *Nature*, 611(7935):365–373, 2022.

[161] Erdinc Sezgin, Ilya Levental, Satyajit Mayor, and Christian Eggeling. The mystery of membrane organization: composition, regulation and roles of lipid rafts. *Nature Reviews Molecular Cell Biology*, 18(6):361–374, 2017.

[162] Bruno Zappone, Vincenzo Caligiuri, Aniket Patra, Roman Krahne, and Antonio De Luca. Understanding and controlling mode hybridization in multicavity optical resonators using quantum theory and the surface forces apparatus. *ACS Photonics*, 8:3517–3525, 2021.

[163] Aniket Patra, Vincenzo Caligiuri, Bruno Zappone, Roman Krahne, and Antonio De Luca. In-plane and out-of-plane investigation of resonant tunneling polaritons in metal–dielectric–metal cavities. *Nano Letters*, 23(4):1489–1495, 02 2023.

[164] M. C. Marchetti, J. F. Joanny, S. Ramaswamy, T. B. Liverpool, J. Prost, Madan Rao, and R. Aditi Simha. Hydrodynamics of soft active matter. *Reviews of Modern Physics*, 85:1143–1189, 2013.